AD-A155 588 IMPACT OF PROPOSED RUNWAY EXTENSION AT LITTLE ROCK MUNICIPAL AIRPORT ON W.. (U) ARMY ENGINEER WATERWAYS EXPERIMENT STATION VICKSBURG MS HYDRA.. 1/1

UNCLASSIFIED J P STEWART ET AL. MAY 85 WES/MP/HL-85-3 F/G 13/2 NL

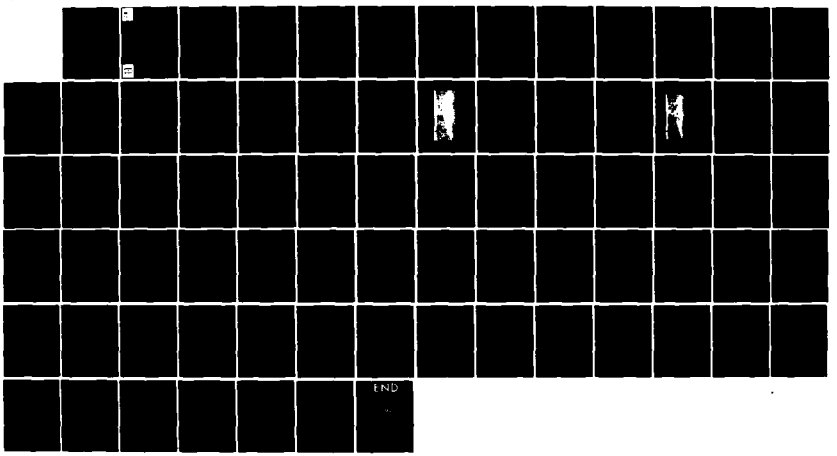

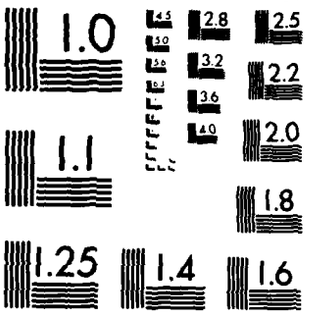

US Army Corps of Engineers



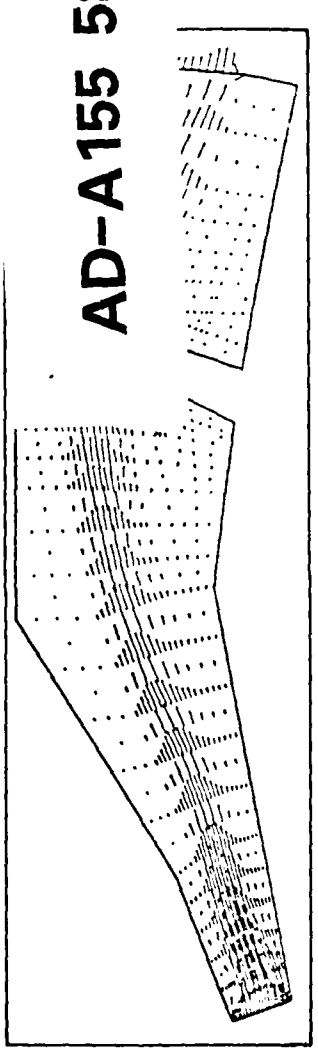

HYDRAULICS LABORATORY



MISCELLANEOUS PAPER HL-85-3

(2)

# IMPACT OF PROPOSED RUNWAY EXTENSION AT LITTLE ROCK MUNICIPAL AIRPORT ON WATER-SURFACE ELEVATIONS AND NAVIGATION CONDITIONS IN ARKANSAS RIVER

by

J. Phillip Stewart, Larry L. Daggett, Robert F. Athow

Hydraulics Laboratory

DEPARTMENT OF THE ARMY
Waterways Experiment Station, Corps of Engineers
PO Box 631
Vicksburg, Mississippi 39180-0631


May 1985
Final Report





Prepared for

US Army Engineer District, Little Rock
Little Rock, Arkansas 72203

Destroy this report when no longer needed. Do not return it to the originator.

The findings in this report are not to be construed as an official Department of the Army position unless so designated by other authorized documents.

The contents of this report are not to be used for advertising, publication, or promotional purposes. Citation of trade names does not constitute an official endorsement or approval of the use of such commercial products.

Unclassified
SECURITY CLASSIFICATION OF THIS PAGE (When Data Entered)

| REPORT DOCUMENTATION PAGE | READ INSTRUCTIONS BEFORE COMPLETING FORM |
|---|---|
| 1. REPORT NUMBER<br>Miscellaneous Paper HL-85-3 | 2. GOVT ACCESSION NO. A155588 / 3. RECIPIENT'S CATALOG NUMBER |
| 4. TITLE (and Subtitle)<br>IMPACT OF PROPOSED RUNWAY EXTENSION AT LITTLE ROCK MUNICIPAL AIRPORT ON WATER-SURFACE ELVATIONS AND NAVIGATION CONDITIONS IN ARKANSAS RIVER | 5. TYPE OF REPORT & PERIOD COVERED<br>Final Report<br>6. PERFORMING ORG. REPORT NUMBER |
| 7. AUTHOR(s)<br>J. Phillip Stewart Larry L. Daggett<br>Robert F. Athow | 8. CONTRACT OR GRANT NUMBER(s) |
| 9. PERFORMING ORGANIZATION NAME AND ADDRESS<br>US Army Engineer Waterways Experiment Station<br>Hydraulics Laboratory<br>PO Box 631, Vicksburg, Mississippi 39180-0631 | 10. PROGRAM ELEMENT, PROJECT, TASK AREA & WORK UNIT NUMBERS |
| 11. CONTROLLING OFFICE NAME AND ADDRESS<br>US Army Engineer District, Little Rock<br>PO Box 867<br>Little Rock, Arkansas 72203 | 12. REPORT DATE<br>May 1985<br>13. NUMBER OF PAGES<br>70 |
| 14. MONITORING AGENCY NAME & ADDRESS(if different from Controlling Office) | 15. SECURITY CLASS. (of this report)<br>Unclassified<br>15a. DECLASSIFICATION/DOWNGRADING SCHEDULE |

16. DISTRIBUTION STATEMENT (of this Report)

Approved for public release; distribution unlimited.

17. DISTRIBUTION STATEMENT (of the abstract entered in Block 20, if different from Report)

18. SUPPLEMENTARY NOTES

Avaliable from National Technical Information Service, 5285 Port Royal Road, Springfield, Va. 22161

19. KEY WORDS (Continue on reverse side if necessary and identify by block number)

Airports--Arkansas--Little Rock (LC)
Airports--Runways (LC)
Arkansas River--Navigation (LC)
Finite element method (LC)
Hydrodynamics (LC)
Navigation--Arkansas River (LC)
Sediment transport (LC)

20. ABSTRACT (Continue on reverse side if necessary and identify by block number)

A 2-D numerical hydrodynamic model was coupled with a 2-D numerical sediment transport model to predict the impact of a proposed runway extension on water-surface elevations in the Arkansas River at Little Rock, Arkansas. The hydrodynamic results were also used as input data to a ship simulator to predict the impact of the proposed runway on navigation characteristics.

The proposed runway will have a noticeable effect on the water-surface
(Continued)

DD FORM 1 JAN 73 1473 EDITION OF 1 NOV 65 IS OBSOLETE

Unclassified
SECURITY CLASSIFICATION OF THIS PAGE (When Data Entered)

20. ABSTRACT (Continued).

profile in the study reach. However, the increased head loss will not violate the 0.5 ft-maximum swellhead criterion. Velocities at and downstream of the constriction will increase approximately 1 fps, or at least 10 percent. While there are some effects on navigation observed due to the proposed project, there does not appear to be any significant increase in navigation difficulty due to the runway extension.

# PREFACE

The work described herein was performed by the US Army Engineer Waterways Experiment Station (WES) with funding by the US Army Engineer District, Little Rock. The numerical models STUDH and RMA-2V and their several utility computer codes were developed with funds from the US Army Engineer District, Portland, and the Chief of Engineers Improvement of Operations and Maintenance Techniques research program.

Personnel of the WES Hydraulics Laboratory performed this study under the direction of Messrs. H. B. Simmons and F. A. Herrmann, Jr., former and present Chiefs of the Hydraulics Laboratory, and M. B. Boyd, Chief of the Hydraulics Analysis Division. Mr. W. A. Thomas was project manager. Messrs. J. P. Stewart and R. F. Athow, Estuaries Division, performed the numerical model studies. Dr. L. L. Daggett and Mr. B. M. Comes performed the ship simulation study. Messrs. Stewart and Daggett prepared this report.

Commanders and Directors of WES during this study and the preparation and publication of this report were COL Tilford C. Creel, CE, and COL Robert C. Lee, CE. Technical Director was Mr. F. R. Brown.



CONTENTS

CONVERSION FACTORS, NON-SI TO SI (METRIC)
UNITS OF MEASUREMENT

US customary units of measurement used in this report can be converted to metric (SI) units as follows:

| Multiply | By | To Obtain |
|---|---|---|
| cubic feet per second | 0.02831685 | cubic metres per second |
| feet | 0.3048 | metres |
| feet per second | 0.3048 | metres per second |
| miles (US statute) | 1.60934 | kilometres |
| pounds-seconds per square foot | 4.8824 | kilograms-seconds per square metre |
| miles per hour | 1.609344 | kilometres per hour |

# IMPACT OF PROPOSED RUNWAY EXTENSION AT LITTLE ROCK MUNICIPAL AIRPORT ON WATER-SURFACE ELEVATIONS AND NAVIGATION CONDITIONS IN ARKANSAS RIVER

## PART I: INTRODUCTION

### Background

1. On 27 September 1983, the Little Rock Municipal Airport Commission made application for a Department of the Army permit to place fill material and bank stabilization stone on the left bank of Fourche Creek at mile 1.7* and on the right bank of the Arkansas River at mile 161.3 in connection with the construction of the Adams Field Runway 4R-22L, Pulaski County, Arkansas (Figure 1). The runway would be placed on fill material varying in height from approximately 258.0 ft NGVD on the south end to 259.75 ft NGVD on the north end.

### Purpose of Study

2. Personnel of the US Army Engineer Waterways Experiment Station (WES) visited the US Army Engineer District, Little Rock (SWL), and photographed significant features of the study area. Hydraulic and sediment data were obtained to develop and verify the numerical models.

3. The purpose of this study was to determine whether or not the proposed runway will satisfy the established criteria for maximum head loss resulting from construction along the Arkansas River. The maximum allowable swellhead criterion for any new construction is 0.5 ft. An additional objective was to predict changes in navigation characteristics resulting from construction of the new runway.

### Approach

4. The solution recommended to SWL was to design a numerical model of the study area using the TABS-2 system. Recently developed in the WES Hydraulics Laboratory, the TABS-2 offers a unique approach to solving complex water

---

* A table of factors for converting non-SI units of measurement to SI (metric) units is presented on page 3.

resource problems. It is a modular system composed of many distinct computer programs linked together by pre- and postprocessors. Each of the major computer programs solves a particular type of problem--hydrodynamics, water quality, or sediment transport. If a new program is needed for a particular application or if new, state-of-the-art programs become available, the modular construction of TABS-2 allows these new programs to be easily incorporated into the system. Thus the modeler is assured of using the best available tools to solve the problem.

5. The two numerical models used in the head loss portion of the study were "A Two-Dimensional Finite Element Program for Problems in Horizontal Free Surface Hydromechanics" (RMA-2V) and "Sediment Transport in Unsteady, Two-Dimensional Flows Horizontal Plane" (STUDH). Both programs employ the finite element method to solve the governing equations. A brief description of RMA-2V and STUDH appears in Appendices B and C, respectively. The ship hydrodynamics model used to predict changes in navigation characteristics was developed by Hydronautics, Inc., and incorporated into the WES ship/tow simulator facility. Appendix D describes this model.

6. The proposed study plan consisted of seven steps:

   a. Develop a finite element grid with a downstream boundary at the I-440 Bridge and an upstream boundary at the M-P Railroad bridge.

   b. Use the computer program (RMA-2V) to calculate flow patterns and water-surface elevations for base conditions and also for the plan condition with the proposed runway. This fixed-bed numerical model would be calibrated for base conditions using SWL's water-surface profile for the Standard Project Flood (SPF) of 625,000 cfs, and verified to the profile of the Navigation Design Flood (NDF) of 310,000 cfs.

   c. Use the flow field for the SPF computed in b as input to (STUDH). This model will predict the new riverbed elevations resulting from the SPF.

   d. Rerun the hydrodynamic model using the updated bed elevations to determine water-surface elevations during the SPF under base conditions.

   e. Repeat steps c and d for the plan condition--i.e., with the proposed runway in the grid--and compare the water-surface elevations with those for the base conditions.

   f. Run the hydrodynamic code for the NDF under base and plan conditions.

   g. Use the results of f to run the WES ship simulation model and compare navigation characteristics under base and plan conditions.

## PART II: THE HEAD LOSS STUDY (Q = 625,000 cfs)

### The Hydrodynamic Model

7. Data requirements for the hydrodynamic model include:

a. The computational grid.

b. Roughness coefficients.

c. Turbulent exchange coefficients.

d. Boundary conditions.

e. Initial water-surface elevation.

8. The computational grid used by RMA-2V and STUDH is created by a pre-processor code, GFGEN. In addition to a title card and run control data, input to GFGEN consists of an element connection table that identifies the nodes defining each element and a list of x- and y-coordinates and bed elevations for every corner node in the grid. The program then computes coordinates and bed elevations for the midside nodes, computes slopes for all boundary nodes, generates plots of the grid, and writes the geometry file used by RMA-2V and STUDH.

9. For this study, an automatic grid generator was used to create the element connection table and nodal x- and y-coordinates for input to GFGEN. Input to the grid generator consisted of sufficient coordinate locations for each row and column to define the geometry of the study area. Rows were aligned along contour lines and columns, along pile dikes. The program then created the element connection table and corner node coordinates. Elevation data were obtained from 1978 sediment range surveys that were transferred to the aerial mosaic and contoured. A plot of the grid was overlaid on the mosaic and elevations were determined at each corner node. The final grid for the base test contained 316 elements and 1,009 nodes (Figure 2). For the plan test, the elements defining the runway were removed from the grid (Figure 3). Initial bathymetry is shown in Figure 4.

10. Manning's n values and the turbulent exchange coefficients were input by element type. The computational grid was partitioned into three regions as shown in Figure 5. The overbank areas with thick grass, trees, and debris were assigned an n-value of 0.060 and a turbulent exchange coefficient of 100 lb-sec/ft$^2$. The areas between pile dikes and along steep elevation gradients were given an n-value of 0.35 and a turbulent exchange coefficient

of 75.0 lb-sec/ft$^2$. The channel elements were assigned an n-value of 0.020 and a turbulent exchange coefficient of 50.0 lb-sec/ft$^2$. The n-values were obtained from 1-D backwater runs provided by SWL. They were adjusted somewhat during the calibration process and are in agreement with values recommended in Chow's Open Channel Flow. The turbulent exchange coefficients were adopted from previous WES model studies using RMA-2V.

11. Boundary condition types for the hydrodynamic model consisted of velocity specifications at the upstream boundary and water-surface elevations at the downstream boundary as shown in Figure 6. Land boundaries were given a slip (parallel) flow specification and nodes along the I-440 embankment were given a zero flow specification. For the SPF discharge of 625,000 cfs, a channel velocity of 11.8 fps was prescribed along the upstream end of the grid and a tailwater of 248.5 ft NGVD was specified at the downstream end. For the navigation design flood, the upstream channel velocity was 8.3 fps and the tailwater elevation was 240.5 ft NGVD. Nonchannel velocity specifications were lowered in proportion to the depth. The velocities selected agreed fairly well with previous studies and yielded the desired discharge.

12. SWL provided water-surface profiles for the two design flows, 310,000 cfs and 625,000 cfs. Since the higher flow was the one of most concern, RMA-2V was calibrated to that flow. The lower discharge was used for verification purposes. The two parameters for calibration were Manning's n and the tailwater elevation. Referring to Figure 5, we reduced the nonchannel n-values from the initial estimates of 0.10 and 0.06 to 0.06 and 0.035, respectively. The channel roughness was not changed. Referring to Figure 6, the tailwater at the downstream boundary of the grid (mile 159.8) was lowered so the computed water-surface elevations tied in to SWL's curve at mile 160.1. Results of the 625,000-cfs calibration are shown in Figure 7. Only the tailwater and upstream velocities were changed for the 310,000-cfs verification run. The resulting profile is shown in Figure 8.

## The Sediment Transport Model

13. The primary objective of this study was to predict the impact of the runway extension on the water-surface profile upstream of the project for a design flood of 625,000 cfs. To accurately predict the water-surface elevations, however, it was first necessary to predict what the bed configuration

would be during such a flood. To do this, the sediment transport model, STUDH, was run for both base and plan conditions.

14. In addition to the hydrodynamic results computed by RMA-2V, the input requirements for the sediment transport model include grain sizes, initial sediment concentration throughout the grid, and inflowing sediment concentrations at the upstream boundary.

15. Grain-size information was obtained from the "East Belt Freeway Arkansas River Bridge: Preliminary Report" (Garver and Garver 1977). This report showed an average grain size of 0.12 mm in the south overbank, 0.14 mm in the north overbank, and 0.27 mm in the main channel and stone dike areas. These values were measured at the bridge site. Boring data included in the dike design blueprints showed that typical sediments were poorly graded sand with some gravel. Based on these data, an average grain size of 0.27 mm was selected for the sediment transport model.

16. Initial sediment concentrations and boundary condition concentrations were both obtained from Project Design Memorandum No. 5-3 (USAED, Little Rock, 1960). The rating curve used is shown in Figure 9. This source, rather than more recent measurements, is expected to produce the most likely concentrations when extrapolated to 625,000-cfs flow.

17. The magnitude of bed change computed by STUDH depends upon the duration of the simulation. Since there was not a design hydrograph for the SPF, SWL used the 1957 flood to determine the time between bank-full flow and the peak. This turned out to be 228 hr. The resulting bathymetry for base and plan conditions is shown in Figures 10-13.

## Results

18. The new bathymetry was then input to the hydrodynamic model to compute water-surface elevations. Figures 14-17 show current patterns for the base and plan conditions. In the base test, approximately 12 percent of the flow passed over Gates Island at the site of the proposed runway. The plan condition diverted this water into the main channel, increasing the velocities by 1 fps. The resulting jet lowered the water-surface elevations downstream of the structure for nearly 2 miles. Upstream of the runway, water-surface elevations were raised about 0.1 ft. Figure 18 shows the predicted impact of the runway extension on the water-surface profile of the design flood.

## PART III: THE NAVIGATION STUDY

### The Navigation Model

19. In 1983, tests were conducted on a typical 15-barge tow operating on the Upper Mississippi River to determine the effects of a reduced dredging policy. That study included making a preliminary estimate of the hydrodynamic coefficients of a 15-barge tow and a 6-barge tow. Then a full set of towing tank tests was performed to determine the deepwater hydrodynamic coefficients, the shallow-water adjustments to these coefficients, the bank effects, and the effects of dikes and irregular bottoms (e.g., large sand waves). It was found that the estimation of the deepwater effects for the tow were reasonably accurate; however, there were not sufficient data on which to base the estimates of the shallow-water and bank effects. Data were available for deep-draft vessels, principally tankers, but the behavior of shallow-draft tows was found to be significantly different. The effects of dikes and irregular bottoms were not significant enough to warrant detailed modeling. Those simulated tows were extensively tested by river pilots and given high ratings on the realism of their performance in both deep pool and restricted channel conditions.

20. For the purposes of the Little Rock Airport Study, a 6-barge tow with the configuration of 3 wide and 2 long was used. The overall tow length was 530 ft and the beam was 105 ft. This is the assumed makeup of a typical large tow on the McLellan-Kerr Waterway because it readily fits into the 600- by 110-ft locks on the waterway. The towboat characteristics are those of the 3,000- to 3,500-HP class. Since some differences were found between the estimated and the tested 15-barge tow used for the Upper Mississippi study, the estimated 6-barge tow was developed from the tested 15-barge tow by adjusting coefficients based on the procedures developed by Hydronautics, Inc., for estimating the coefficients. This involved adjusting the coefficients according to dimension or mass ratios. The same shallow-water and bank effects were used as determined in the 15-barge tow tests. For the Little Rock simulation, the tow operated in relatively deep water with depth-to-draft ratios of 3 or greater and at large distances from the banks, at least two beam widths. Therefore the shallow-water and bank effects are assumed to be small.

21. Results of standard maneuvering tests for the estimated 6-barge tow

tow used in this study and the tested 15-barge tow are shown in Table 1. As can be seen, the 6-barge tow travels at a faster rate than the heavier 15-barge tow and stops and turns quicker than the larger tow. In addition, prototype tests have been conducted for a similar size, powered tow but with a different configuration. These tests provide a comparison of the tow speed/power relation. These tows were 3,330- to 2,670-hp towboats and the tow was 1,160 ft long and 54 ft wide. This is about equivalent in carrying capacity to the 3 by 2 tow but is a more slender configuration and, therefore, less resistant.

Table 1

Comparison of Tow Maneuvering Characteristics

| | Estimated 6-Barge Tow | Measured 15-Barge Tow |
|---|---|---|
| 30-deg turning circle | | |
| Advance | 1,779 ft | 3,720 ft |
| Transfer | 885 ft | 1,781 ft |
| Full speed ahead | 9.79 mph | 7.68 mph |
| Crash stop | | |
| Stopping time | 4.10 sec | 14.0 sec |
| Distance | 1,032 ft | 2,509 ft |
| Crash stop with rudder | | |
| Stopping time | 4.10 sec | 14.2 sec |
| Distance | 1,030 ft | 2,577 ft |

The full ahead speed for these tows is 11.6 and 11.9 mph, respectively. The 6-barge tow used for this study falls between the 15-barge tow and the more slender equivalent 6-barge tow as expected. During the test runs, the tow was operated at 90 percent of full throttle which is equivalent to 2,700 hp.

22. The condition selected to test the impacts on navigation due to the constriction of the waterway with the proposed airport extension was the highest flow at which navigation is permitted. This flow is 310,000 cfs and overtops the overbank areas on both sides of the waterway. The airport expansion would then create a blockage to the flow over the Gates Island on the right-hand descending bank and redirect the flow into the navigation channel. At the highest flow under which navigation is permitted, the potential for cross-currents will be the highest and therefore the impacts on navigation will be the greatest.

23. The approach taken in this study was to compare the navigation conditions for the existing, or base, conditions with the conditions created with the airport extension in place, i.e., the plan condition. These conditions were compared for both downbound and upbound transits. Since the airport extension plan does not protrude into the navigation channel per se, the navigation channel dimensions do not change. The only change then is in the current magnitude and direction in the vicinity of the extension. These current patterns were determined using the RMA-2V model using a flow of 310,000 cfs and the appropriate tailwater elevation from SWL's water-surface profiles.

24. The general flow patterns for the base and plan are shown in Figures 19 and 20, respectively. The expanded view of the currents in the vicinity of the airport extension given in Figures 21 and 22 shows in more detail the changes in the flow due to the runway. Changes in the direction of flow are concentrated on the right-hand descending side of the channel and do not appear to extend into the navigation portion of the channel which is on the left-hand side of the channel. There is an increase of 1 to 1.5 fps in the magnitude of the currents in the navigation channel.

25. For purposes of the navigation model, 30 cross sections of velocities and depths were extracted from the RMA-2 model results within the navigation channel. For this purpose, the navigation channel was taken as either the bank line, the 9-ft water depth contour, or the end of the dikes. The actual marked navigation channel lies within this definition. The currents extracted from the RMA-2 results for the base and plan are shown in Figures 23 and 24. Again, the magnified views given in Figures 25 and 26 show that the impact on the currents in the navigation channel is minor and consists of increased velocity magnitudes in the contracted portion of the channel and some limited change in direction immediately below the airport extension. It should be noted that the channel cross sections are concentrated in the area of the planned construction so that these effects are properly modeled for the navigation tests.

26. Figures 27 and 28 show the modeled currents and the navigation channel boundaries for the base and plan conditions, respectively. The dike fields and the airport extension are displayed for reference purposes. The navigation buoys are also included in the figures although they are difficult to distinguish among the current vectors.

27. In order to provide direct comparison of the impacts of the airport extension, the navigation transits were made under the control of an autopilot which is designed to correct for errors or changes in heading and distance off course and to minimize the rate of rotation. An advance look-ahead feature is included that is a function of the magnitude of the heading change in the desired course. Using the autopilot provides a consistent level of control of the tow. Any significant impacts would be expected to be evident in the track lines or in the difficulty of the navigation, e.g., increased rudder activity and/or reduced rudder reserve. The autopilot track lines to be followed, shown in Figures 29 and 30, are identical for base and plan. The track lines in the base condition (Figure 29) are for a downbound transit and the track lines in the plan condition (Figure 30) are for an upbound transit.

## Results

28. The transit paths for the downbound transits of the tow are shown in Figures 31 and 32 for the base and plan conditions, respectively. It can be seen by overlaying these two plots that the path taken by the tow is not significantly affected by the runway. In both cases, the tow has some difficulty in changing course just downstream from the location of the proposed airport extension. The upbound transit track lines are shown in Figures 33 and 34 for the base and plan conditions, respectively. Notice that the upbound tow has more control in making the turns as the changes in the course line are very distinct. The tow is also going much slower as noted by the dense line with small incremental steps of the tow being plotted at constant time intervals. Again, it is difficult to detect any significant differences in the path followed by the upbound tow. The track line is more dense and hence the tow is going slower just downstream of the extension in the plan condition. Also, both upstream transits terminated when the maximum run time was exceeded. The transit through the plan condition is much shorter than the base condition transit. This is an indication of the increase in water velocity in the plan condition.

29. In order to understand the navigation activities required to make these transits, plots of the rudder and engine activities and the tow speed and distance off-track were generated. The plots for the downbound tow for the base and plan condition are shown in Figures 35 and 36, respectively; the

upbound transit activities are shown in Figures 37 and 38. For reference purposes, the navigation mile locations are indicated on the abscissa with triangles beginning with navigation mile 118.0 and proceeding downstream from left to right. Again, it is noted that the downbound transits are proceeding at a much higher speed, approximately 12 to 15 mph, while the upbound transits vary between 1 and 5 mph. Also, the downbound transits require more extensive rudder activity and have larger deviations from the desired track line. However, it is difficult to distinguish any significant differences between the base and plan for transits in the same direction.

30. To assist in this analysis, comparison plots of the clearance to the edge of the navigation channel and of the rudder settings and speed were developed. Figure 39 shows that the downbound transits for the base and plan conditions maintained nearly the same clearances on the port and starboard sides. Differences appear to be 20 ft or less. The upbound transits, shown in Figure 40, may have experienced larger differences between the base and plan conditions with the area between navigation miles 115.0 and 115.5 finding the tow about 30 ft closer to the starboard channel edge with the airport extension in place. However, since there is over 1,000 ft of clearance on the port side there is adequate channel available for the tow to move away from the starboard side.

31. The amount of rudder activity required for both the upbound and downbound tows is nearly the same, as is shown in Figures 41 and 42. In all cases, there is at least 10 deg of rudder reserve remaining for emergency maneuvers and except for a few cases rudder settings are less than 15 deg. The differences in forward speed are evident and the increased current effects on the speed are quite distinct between navigation miles 114.0 and 115.0.

## PART IV: CONCLUSIONS

32. The proposed runway will have a noticeable effect on the water-surface profile in the study reach. However, the increased head loss will not violate the 0.5-ft maximum swellhead criterion. Velocities at and downstream of the constriction will increase approximately 1 fps, or about 10 percent.

33. While there are some effects on navigation observed due to the proposed project, there does not appear to be any significant increase in navigation difficulty due to the airport extension evident in the autopilot runs. There is a distinct decrease in forward speed for upbound tows due to the increased velocities. It is evident from the "full speed ahead" values in Table 1 that for tows of this size, the power of the towboat cannot be any smaller than that used for the model tow. This is true for the existing conditions as well as the proposed runway extension, however.

34. The best data available within time and budgetary constraints have been used and state-of-the-art solution techniques have been applied to predict the impact of the proposed runway on water-surface profiles and navigation characteristics. Results show that the impact will not be significant.

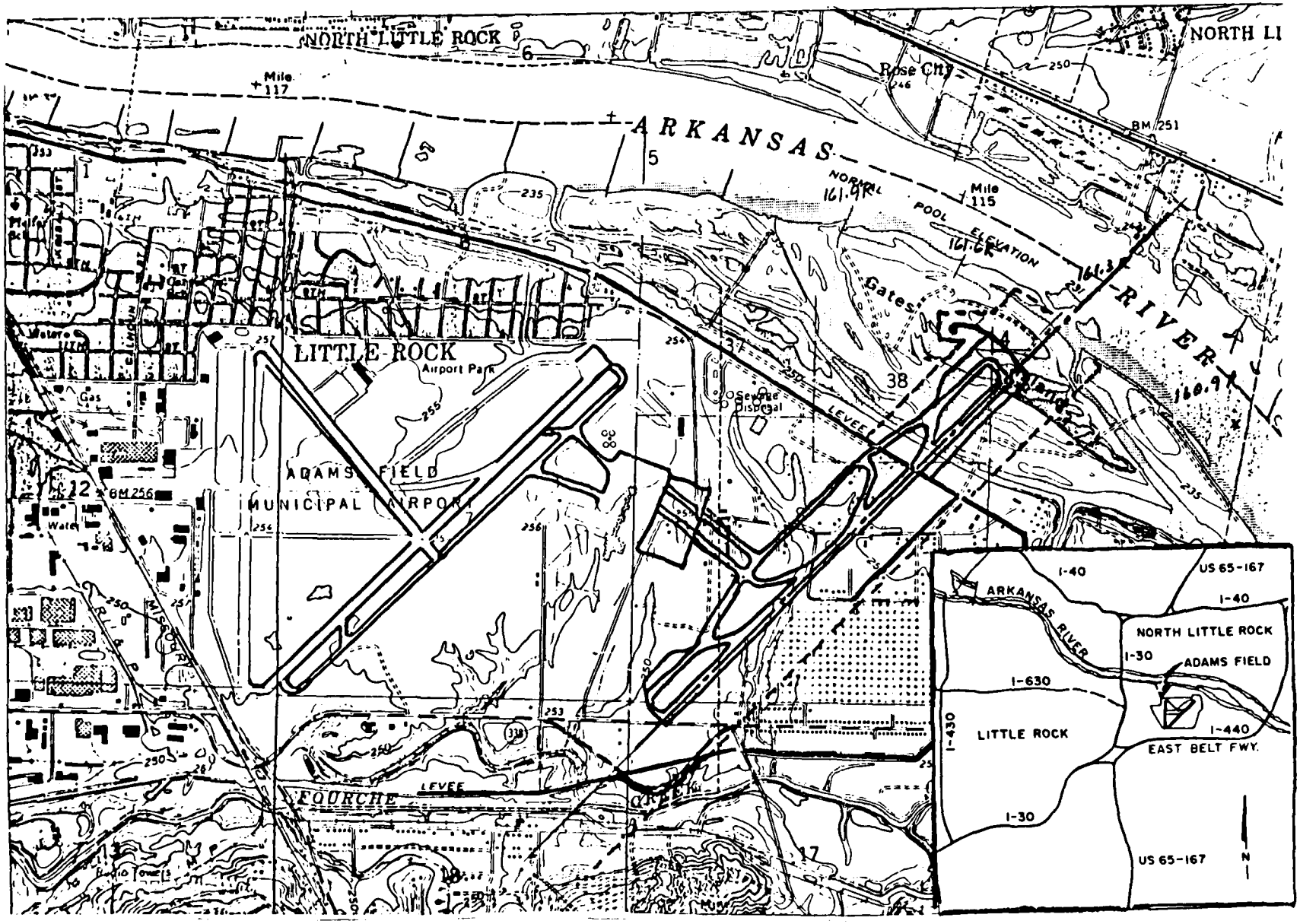


Figure 1. Location map

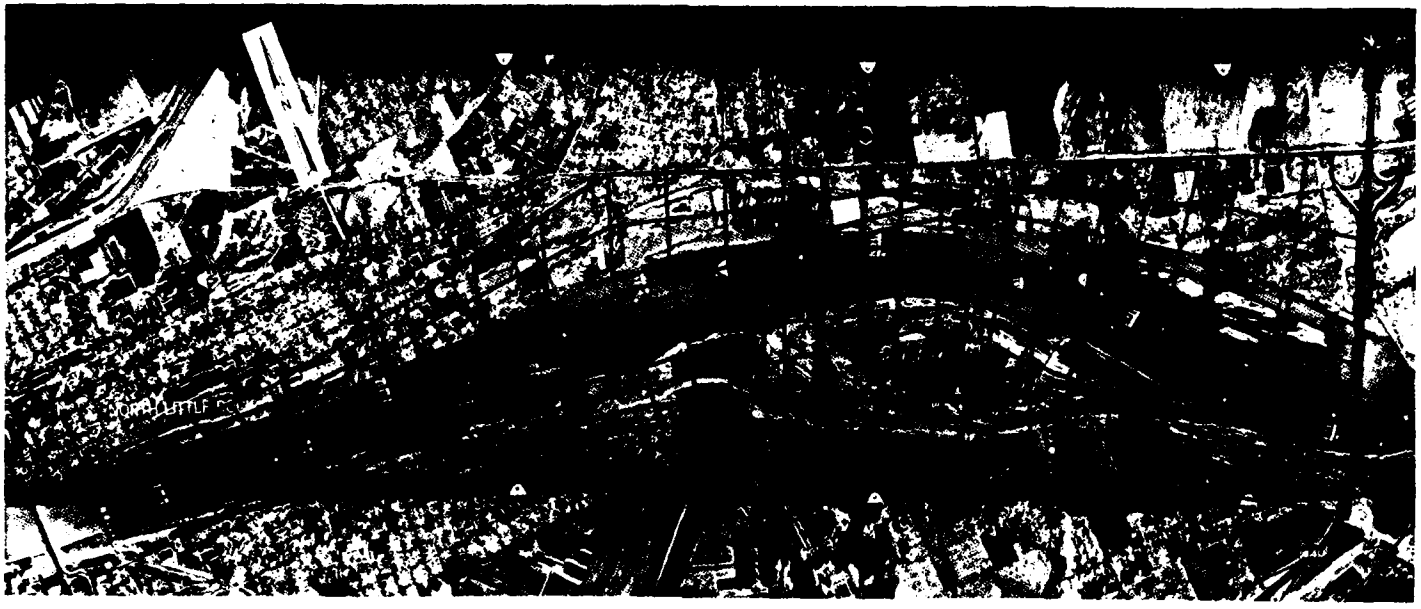

Figure 2. Computational grid for base test

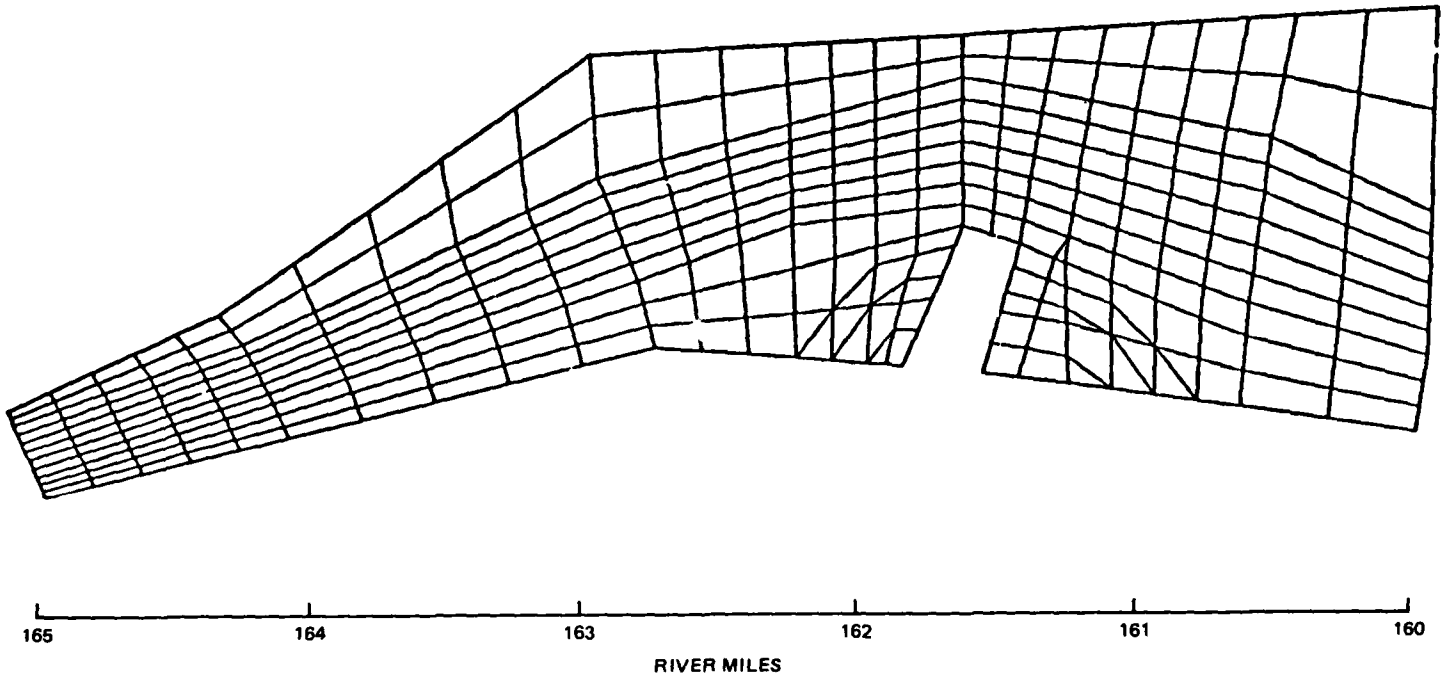


Figure 3. Computational grid for plan test, 625,000 cfs

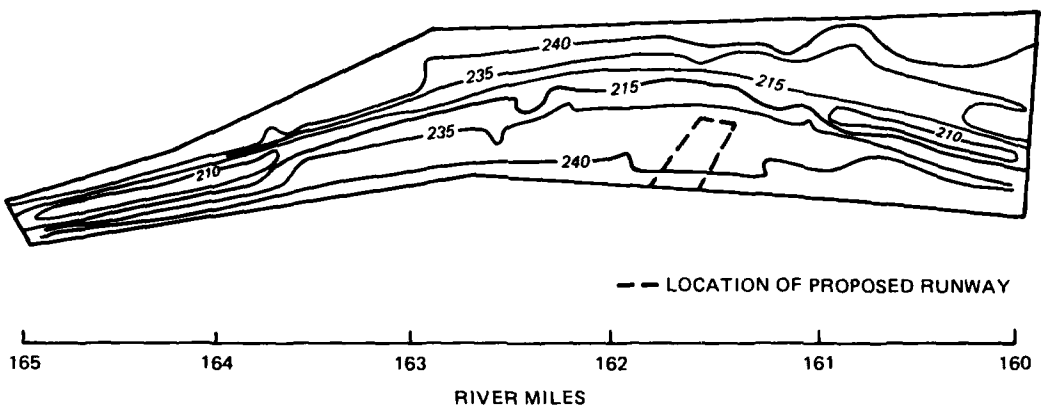


Figure 4. Initial bed elevations

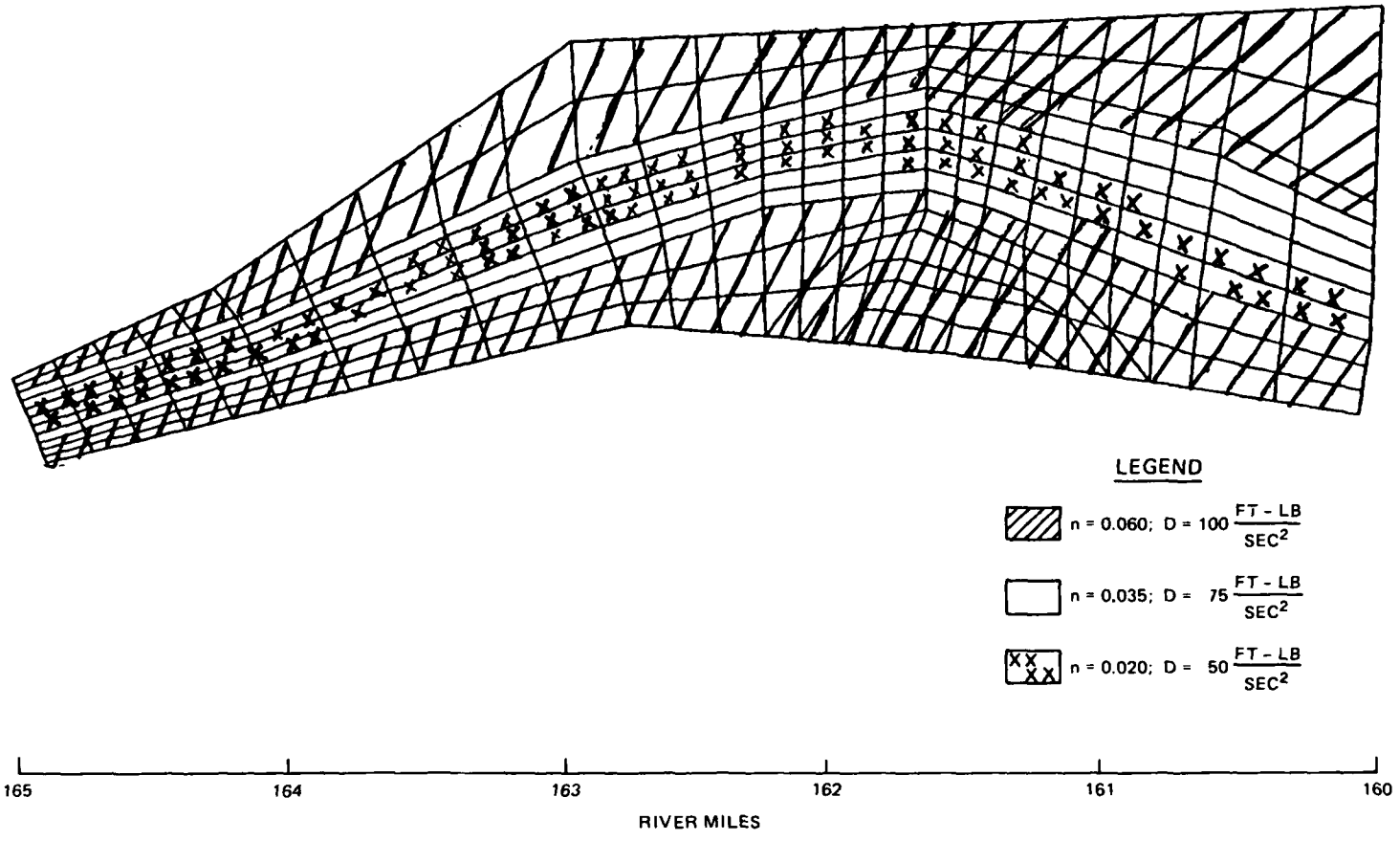


Figure 5. Element types

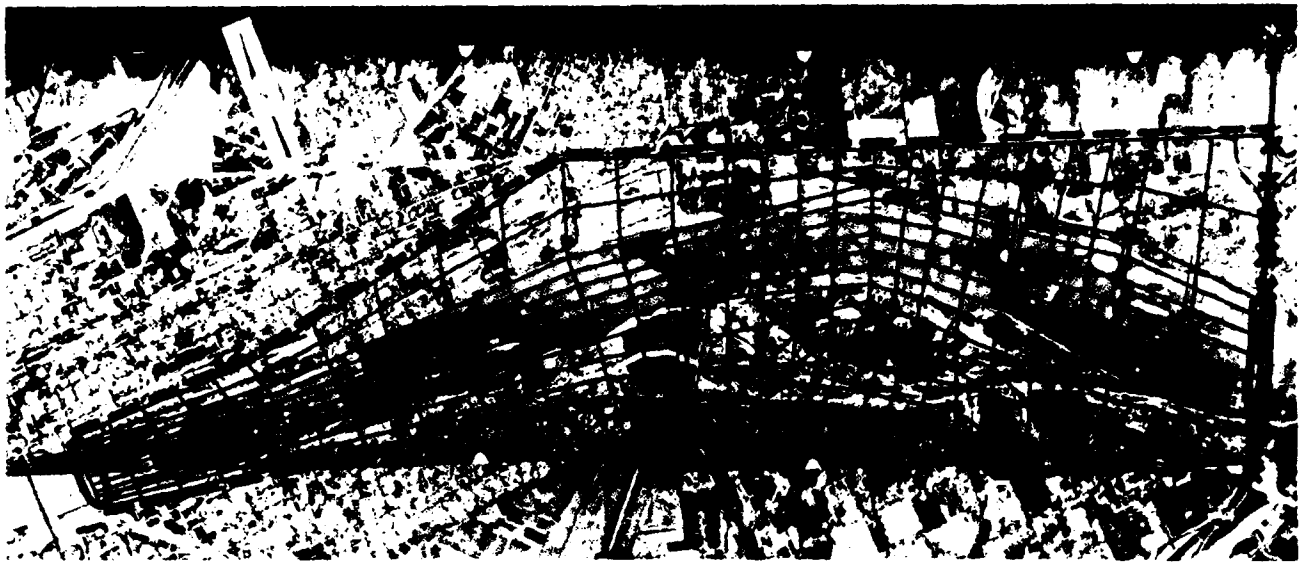

LEGEND

× ZERO FLOW

WATER-SURFACE ELEVATION

VELOCITY

SLIP (PARALLEL)

Figure 6. Boundary condition specification

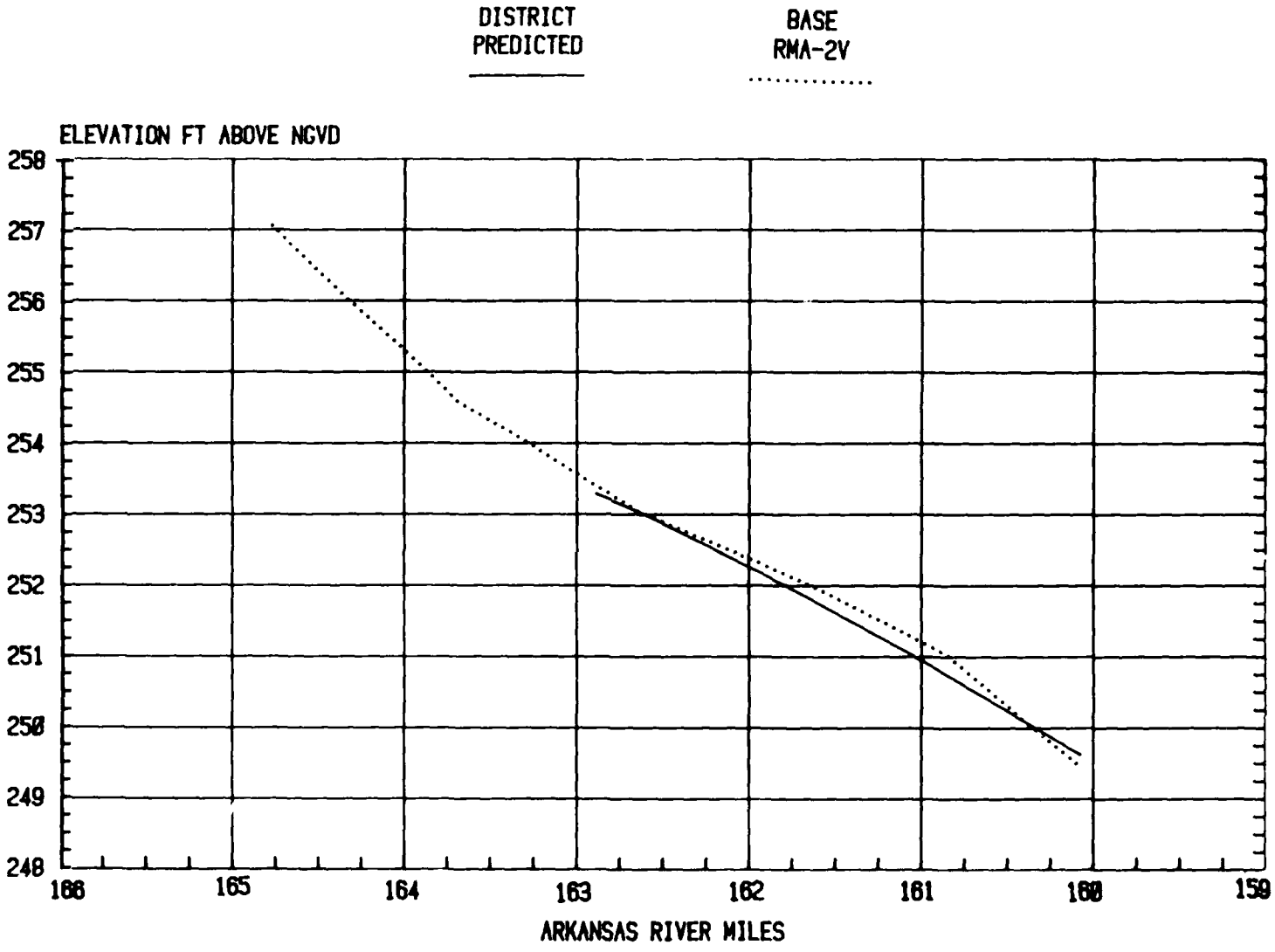


Figure 7. Calibration of RMA-2V

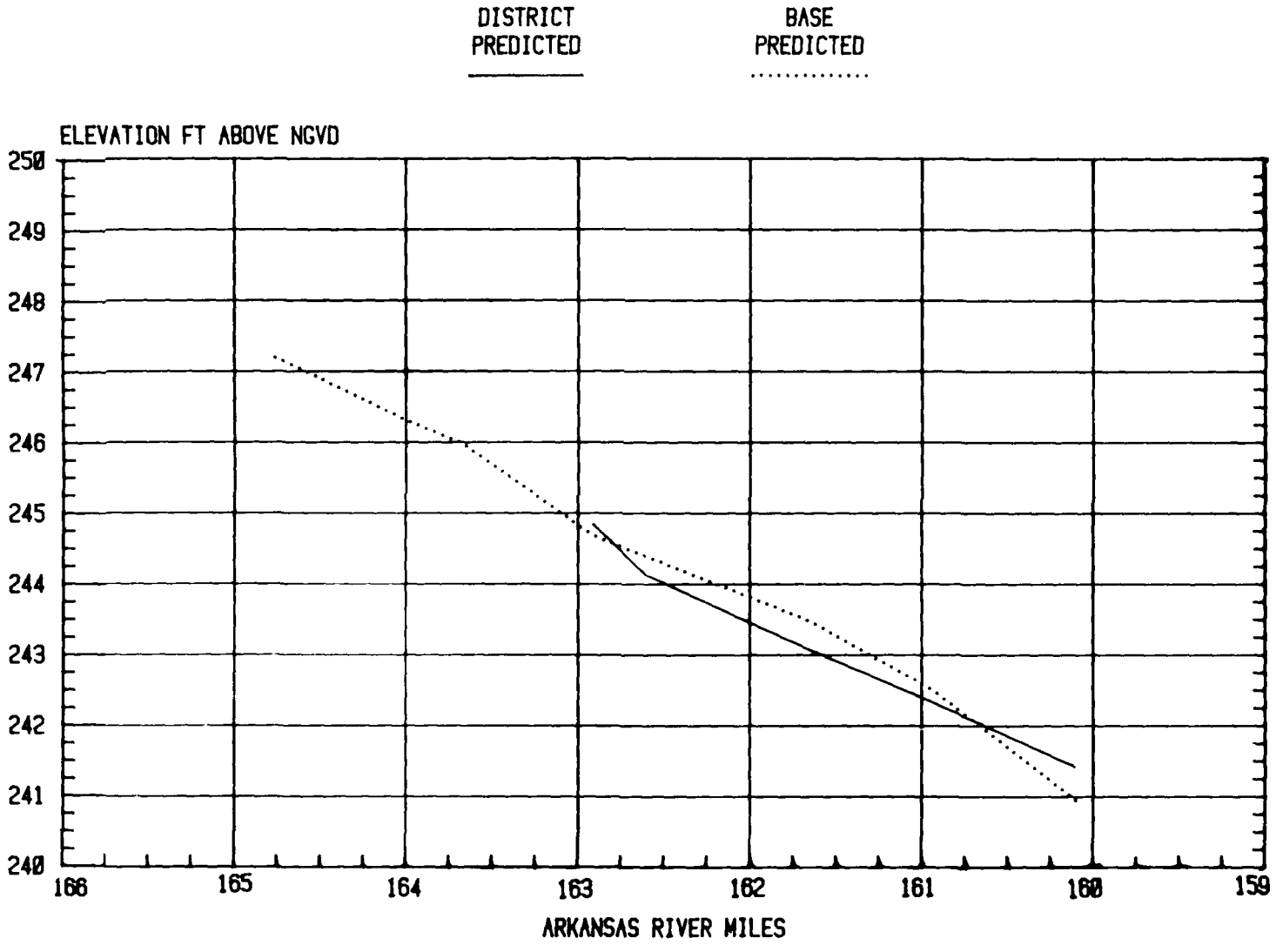


Figure 8. Verification of RMA-2V

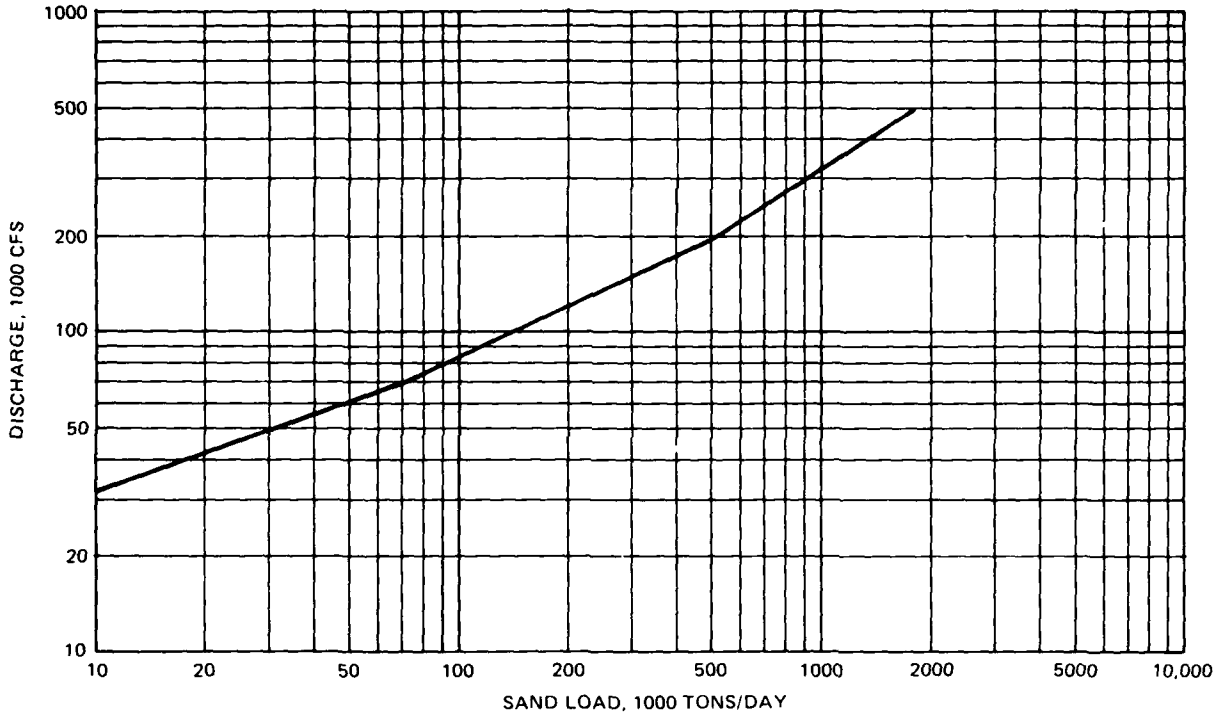


Figure 9. Sediment load rating curve

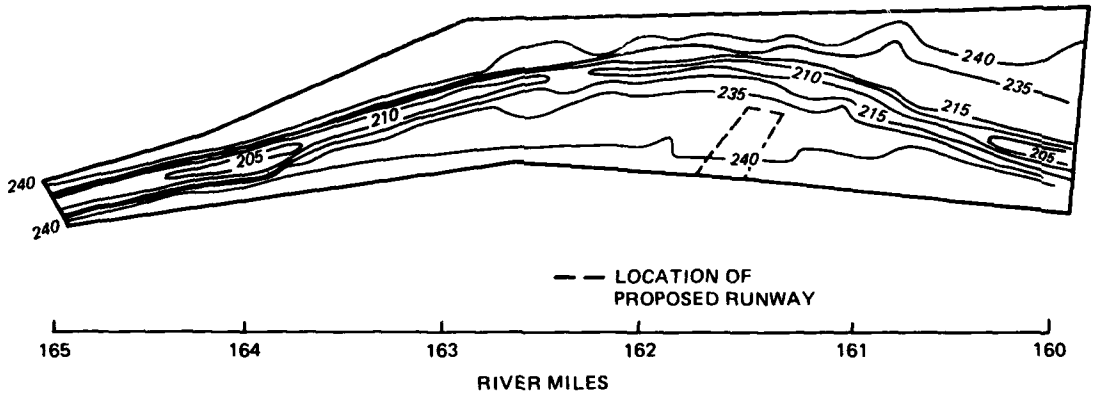


Figure 10. Postflood bathymetry for base test, after 228 hr of sediment transport

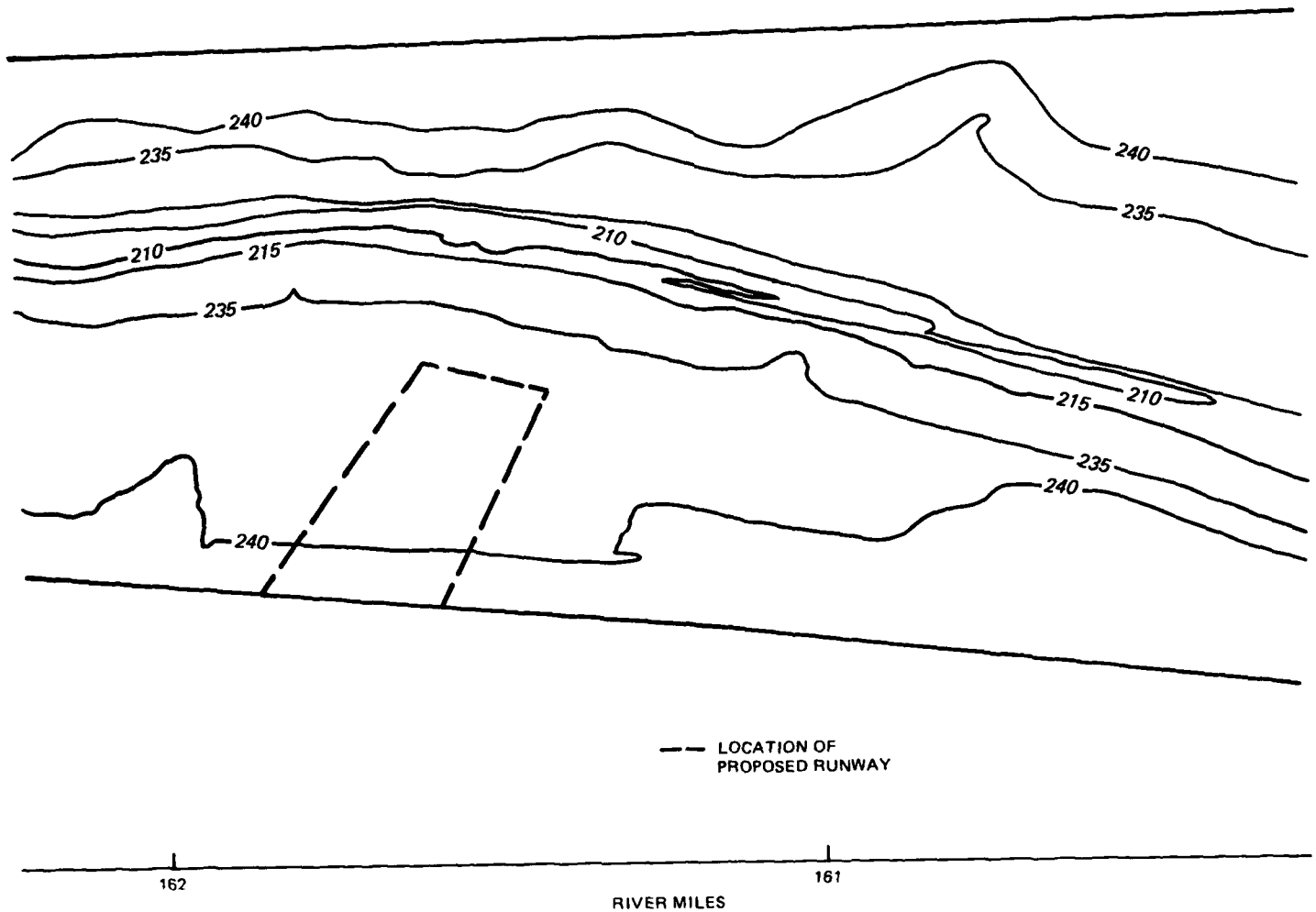


Figure 11. Magnification of postflood bathymetry for base test, after 228 hr of sediment transport

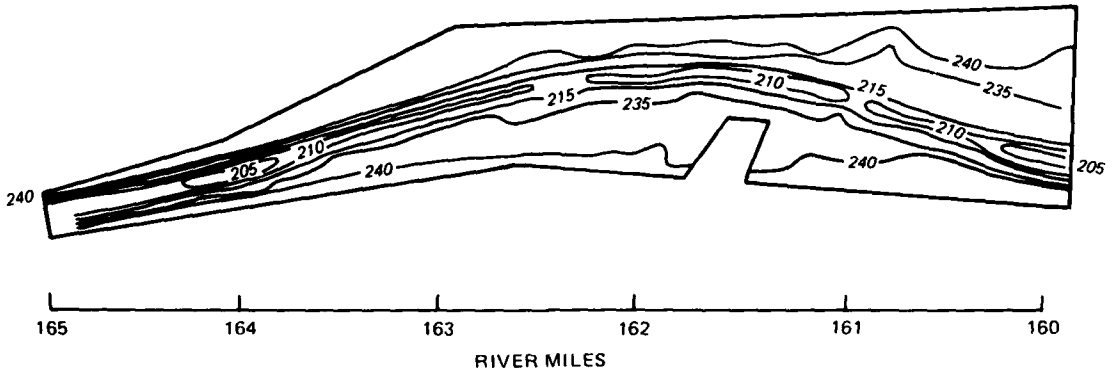


Figure 12. Postflood bathymetry for plan test, after 228 hr of sediment transport

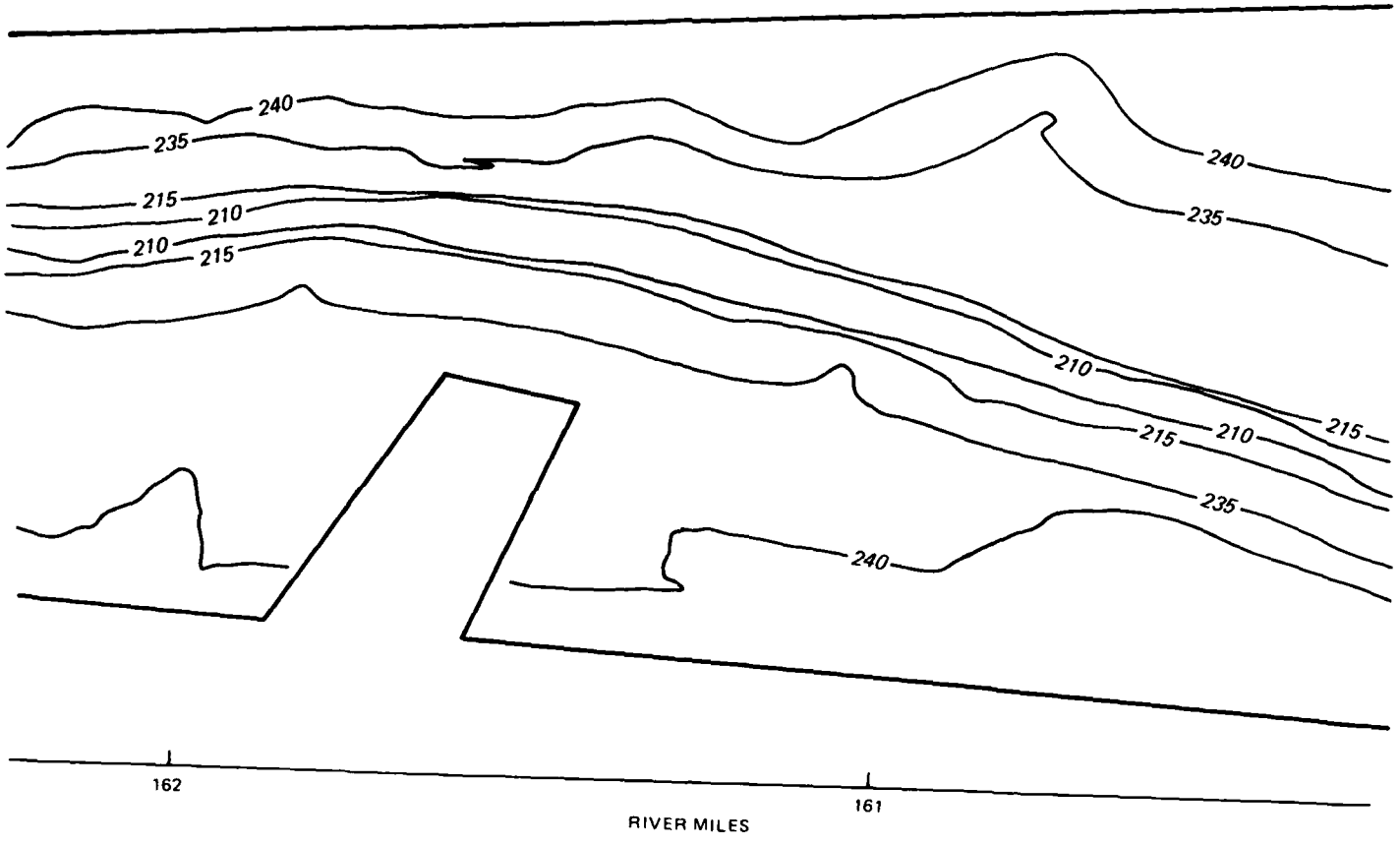


Figure 13. Magnification of postflood bathymetry for plan test, after 228 hr of sediment transport

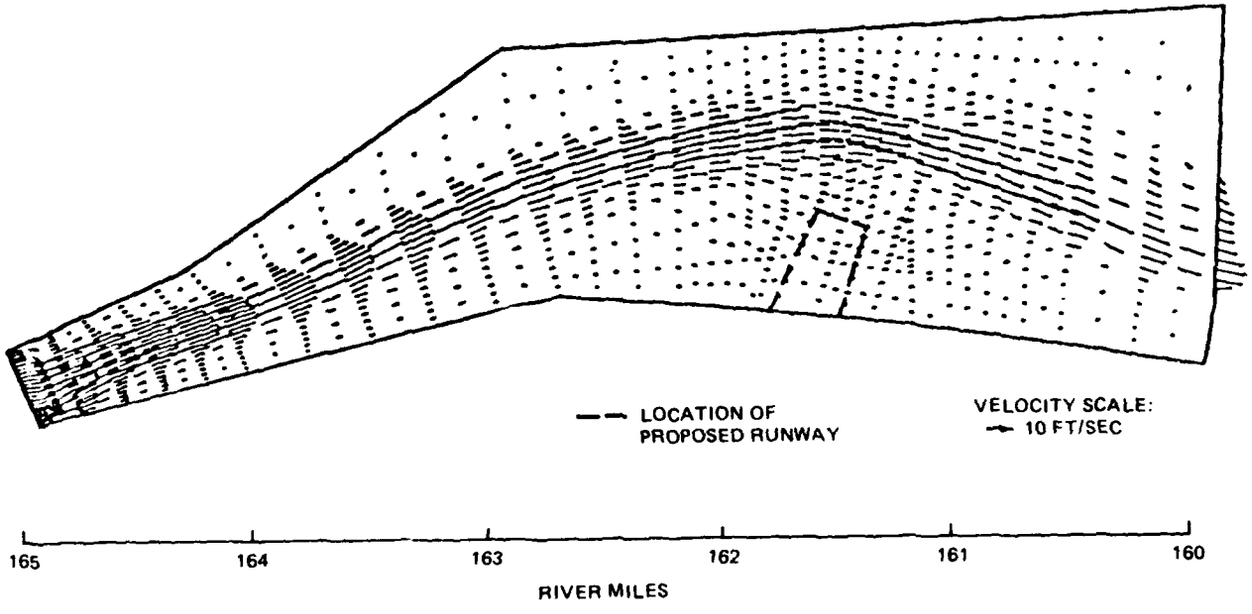


Figure 14. Postflood current patterns for base test, after 228 hr of sediment transport

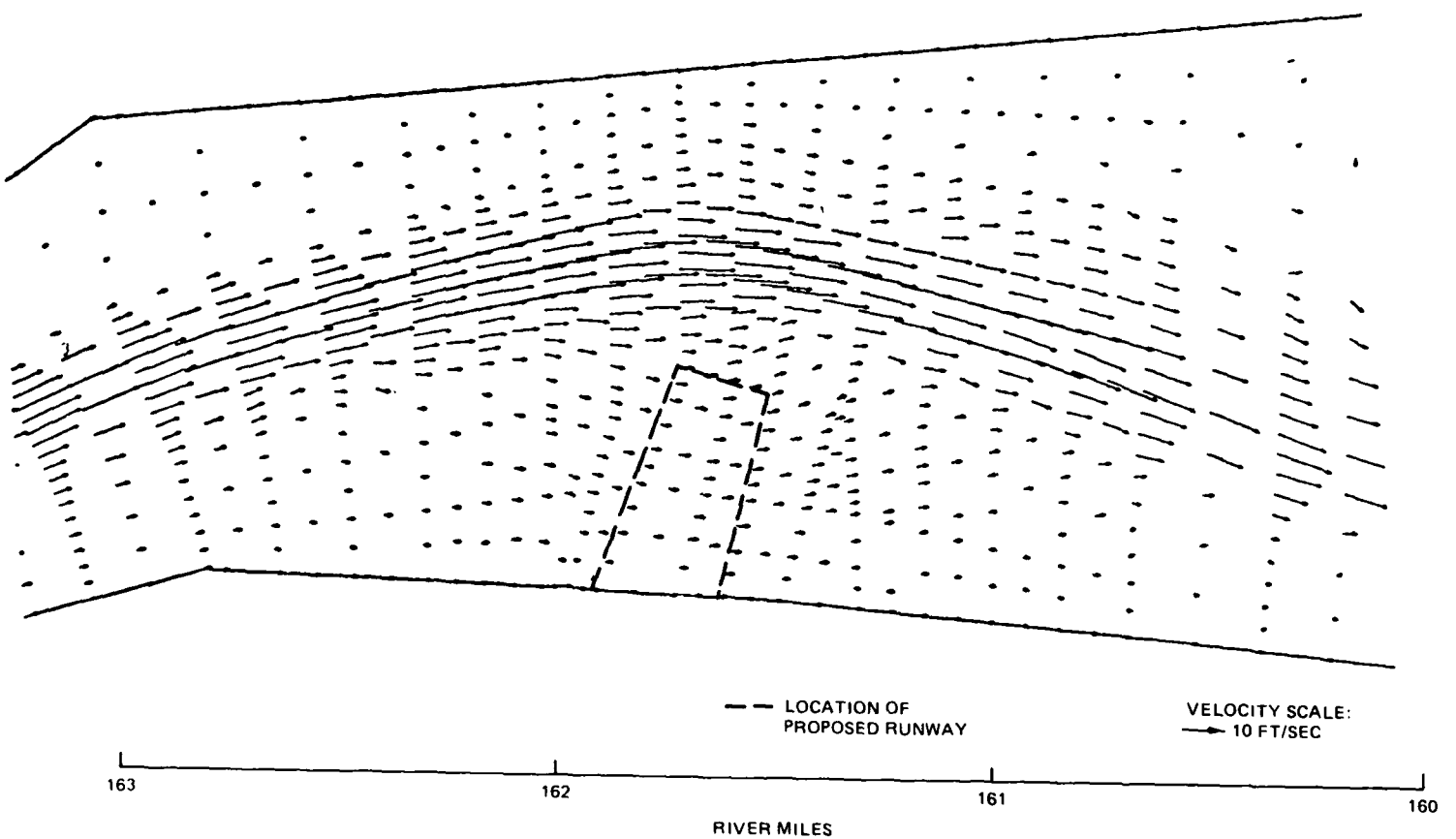


Figure 15. Magnification of postflood current patterns for base test, after 228 hr of sediment transfer

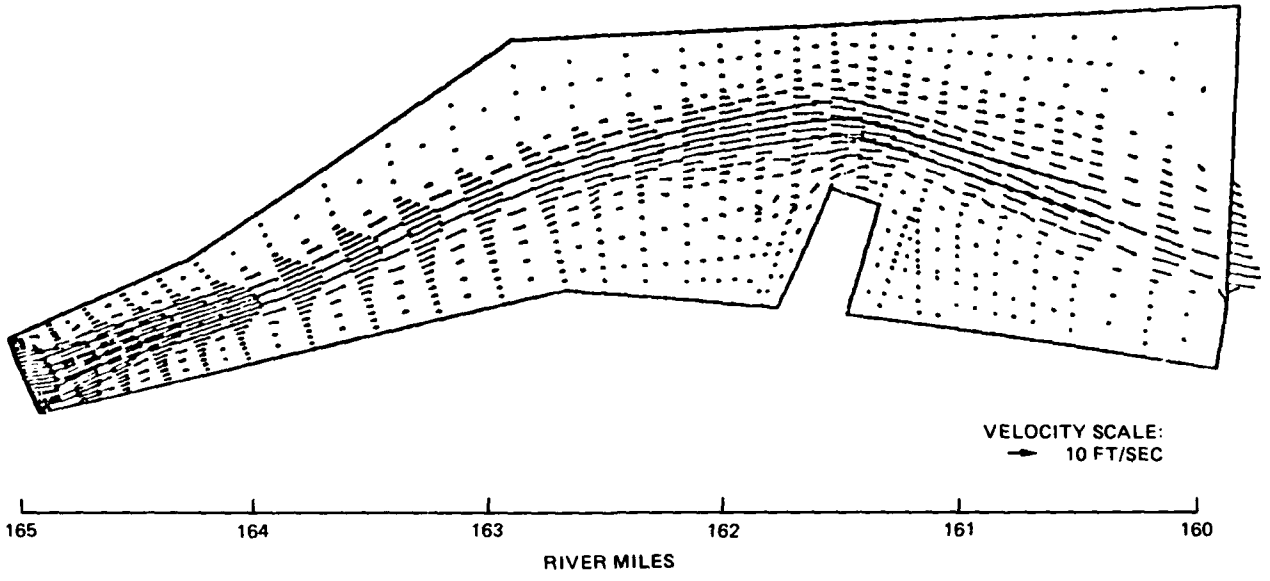


Figure 16. Postflood current patterns for plan test after 228 hours of sediment transport

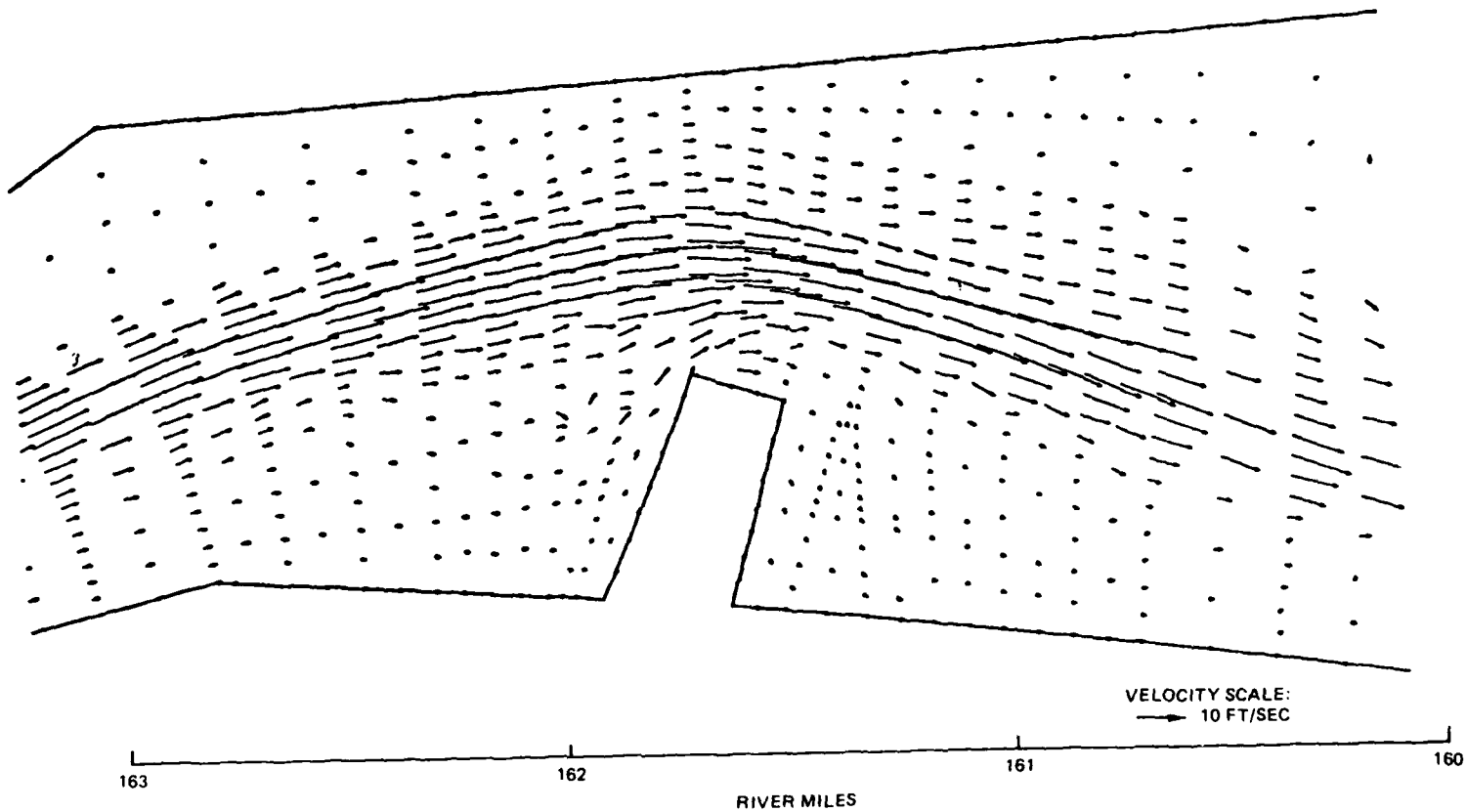


Figure 17. Magnification of postflood current patterns for plan test after 228 hr of sediment transport

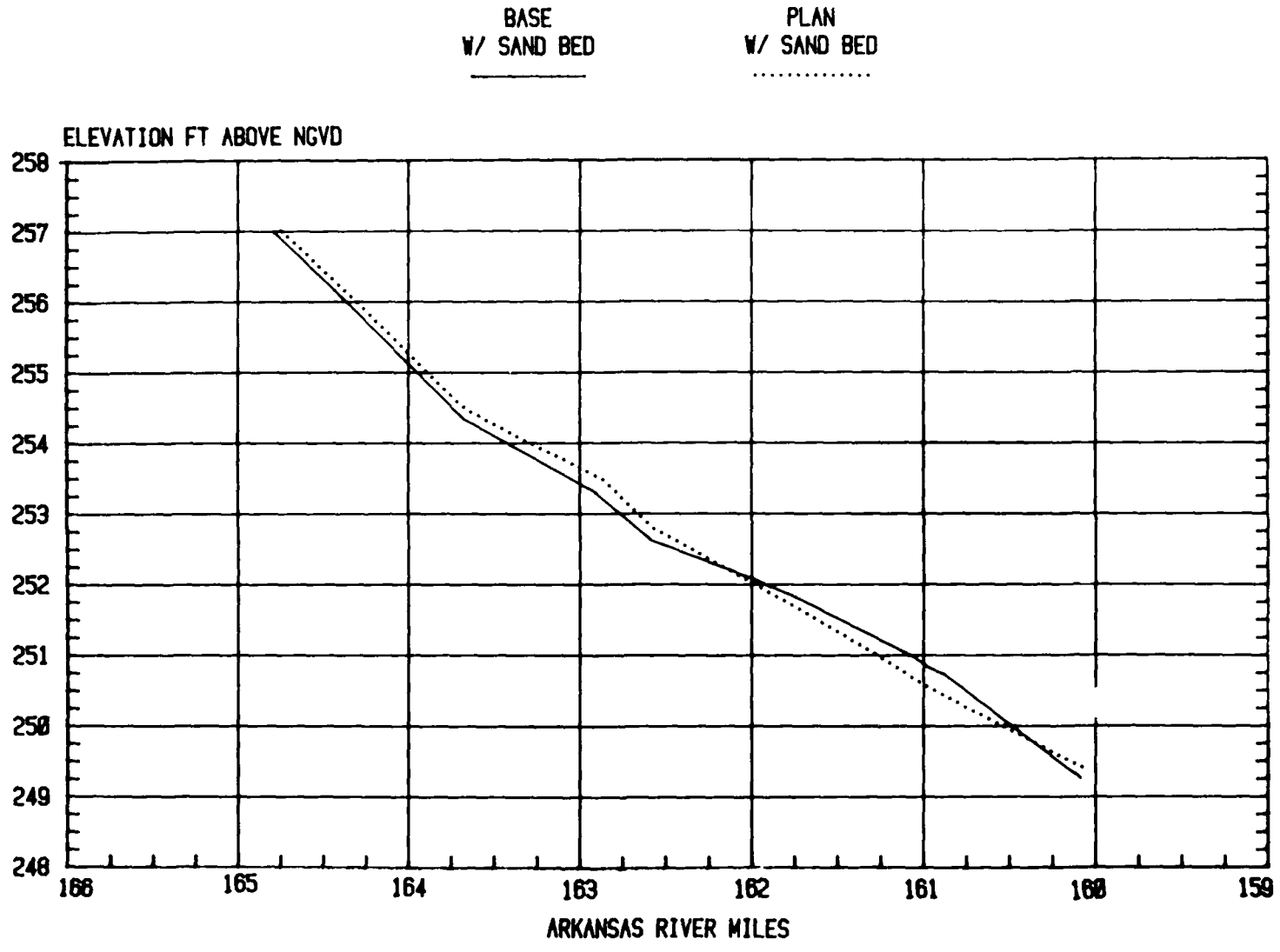


Figure 18. Predicted water-surface profiles for base and plan tests

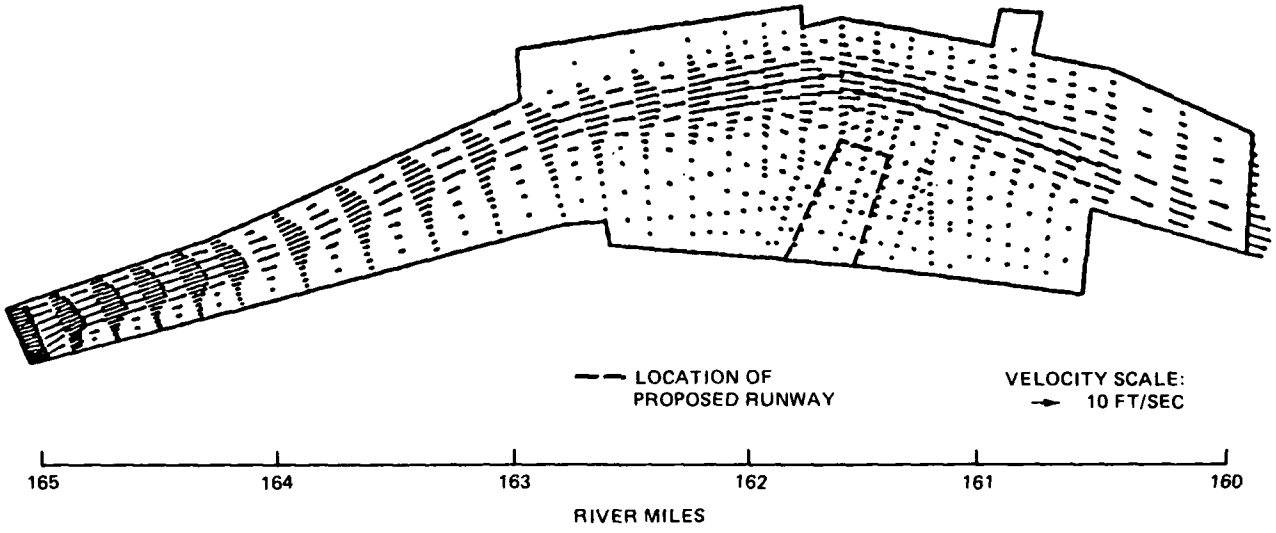


Figure 19. Flow patterns for navigation design flood, base test

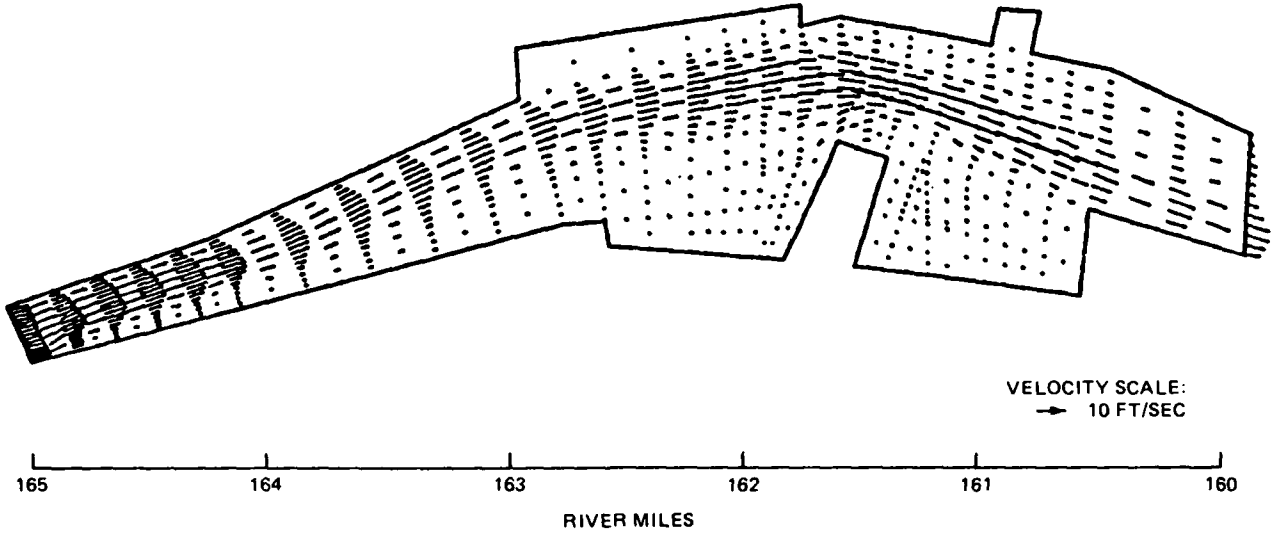


Figure 20. Flow pattern for navigation design flood, plan test

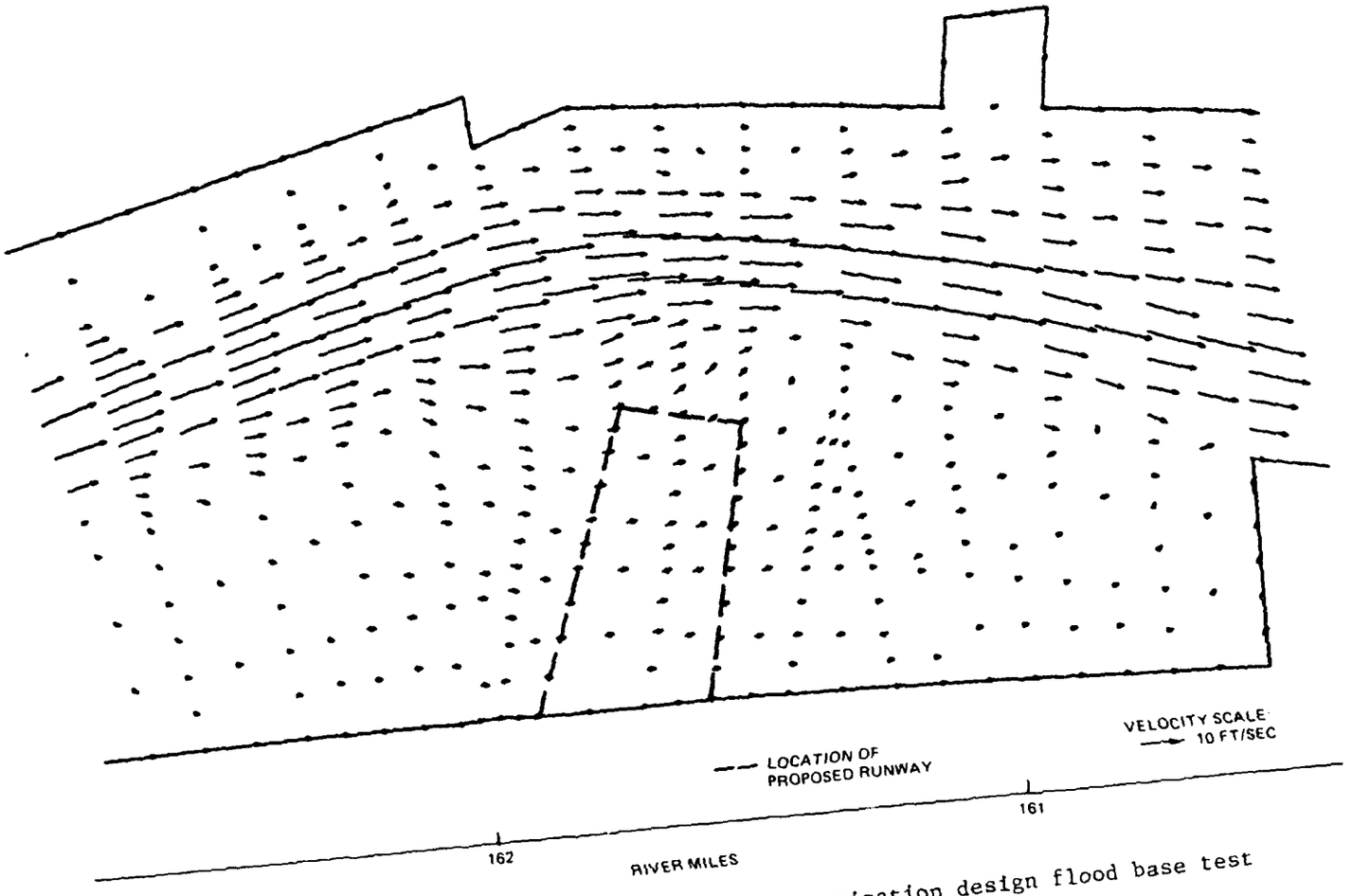


Figure 21. Magnification of flow pattern for navigation design flood base test

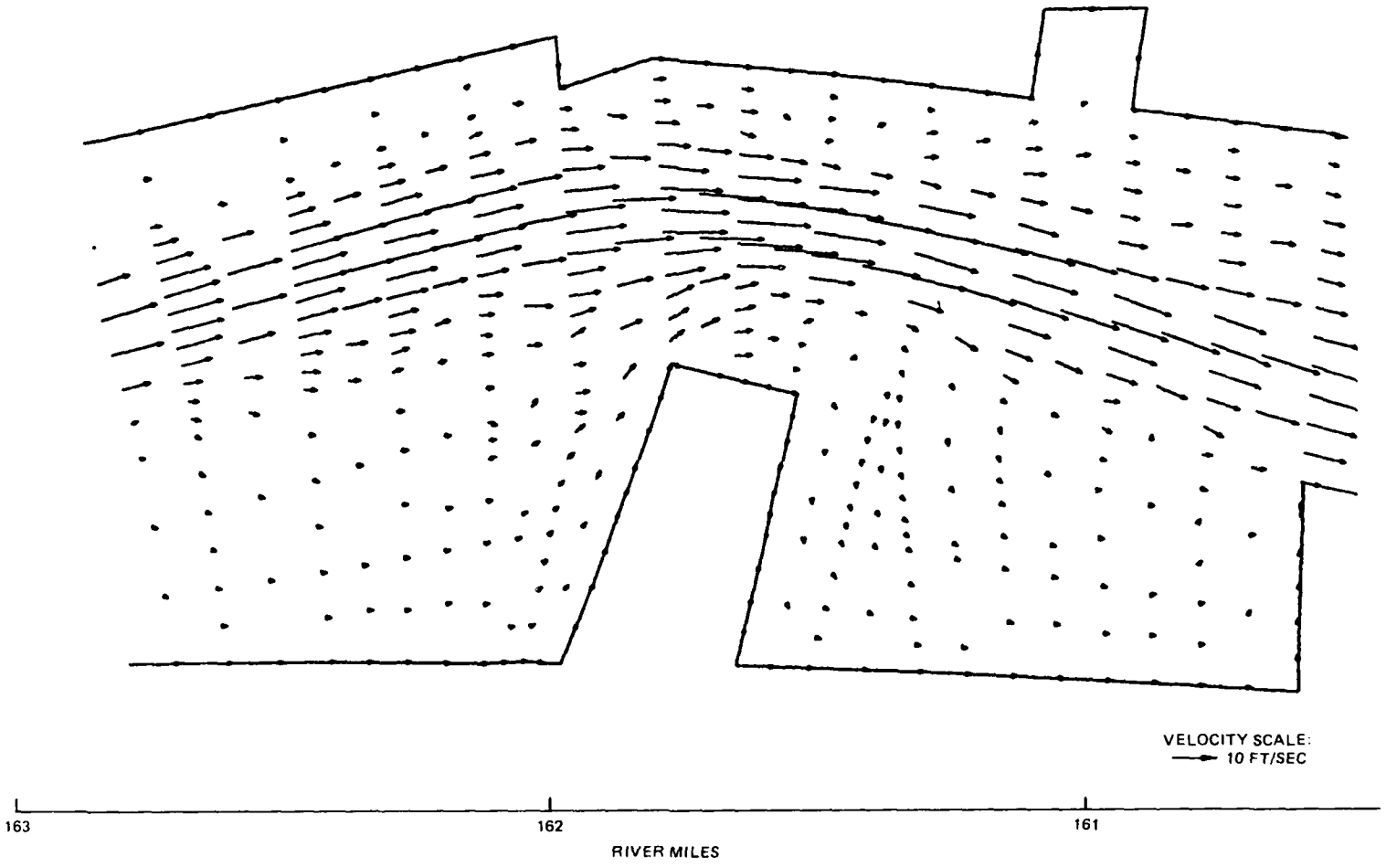


Figure 22. Magnification of flow pattern for navigation design flood plan test

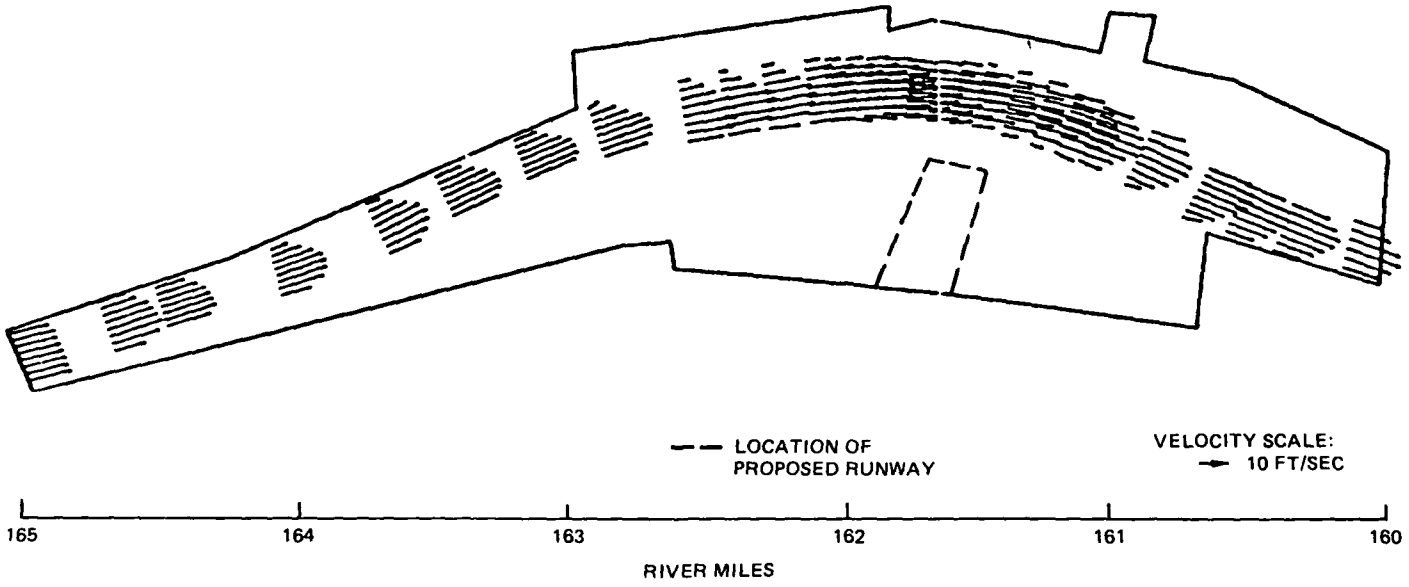


Figure 23. Flow pattern in navigation channel, base test

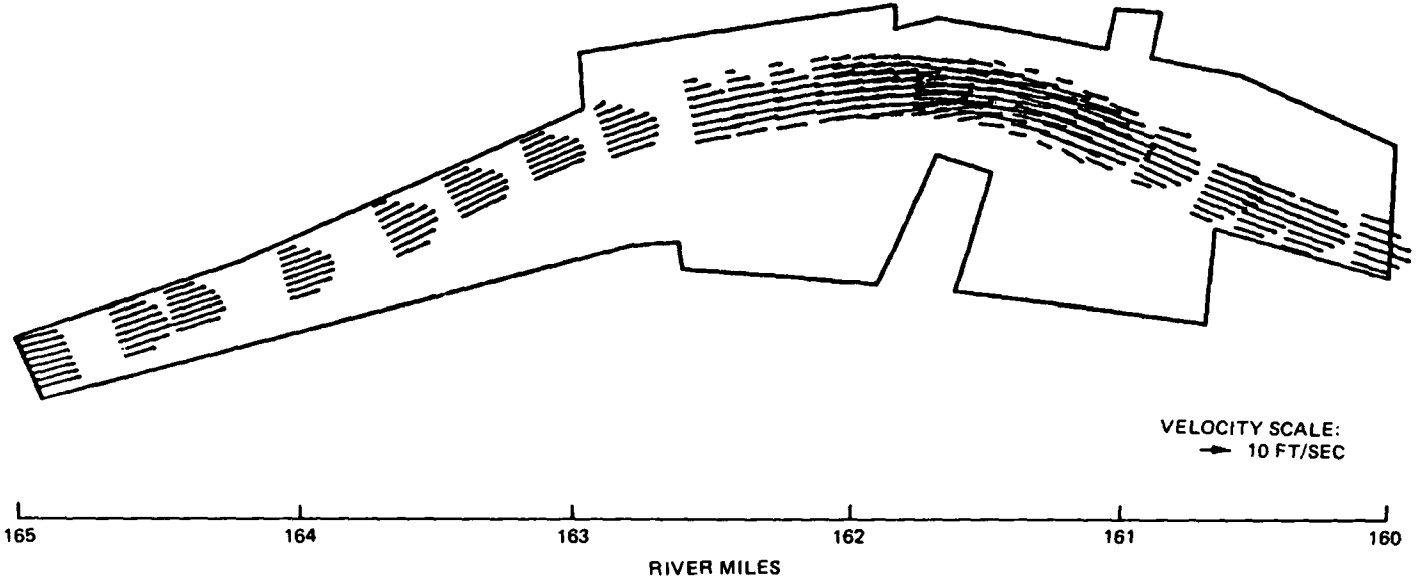


Figure 24. Flow pattern in navigation channel, plan test

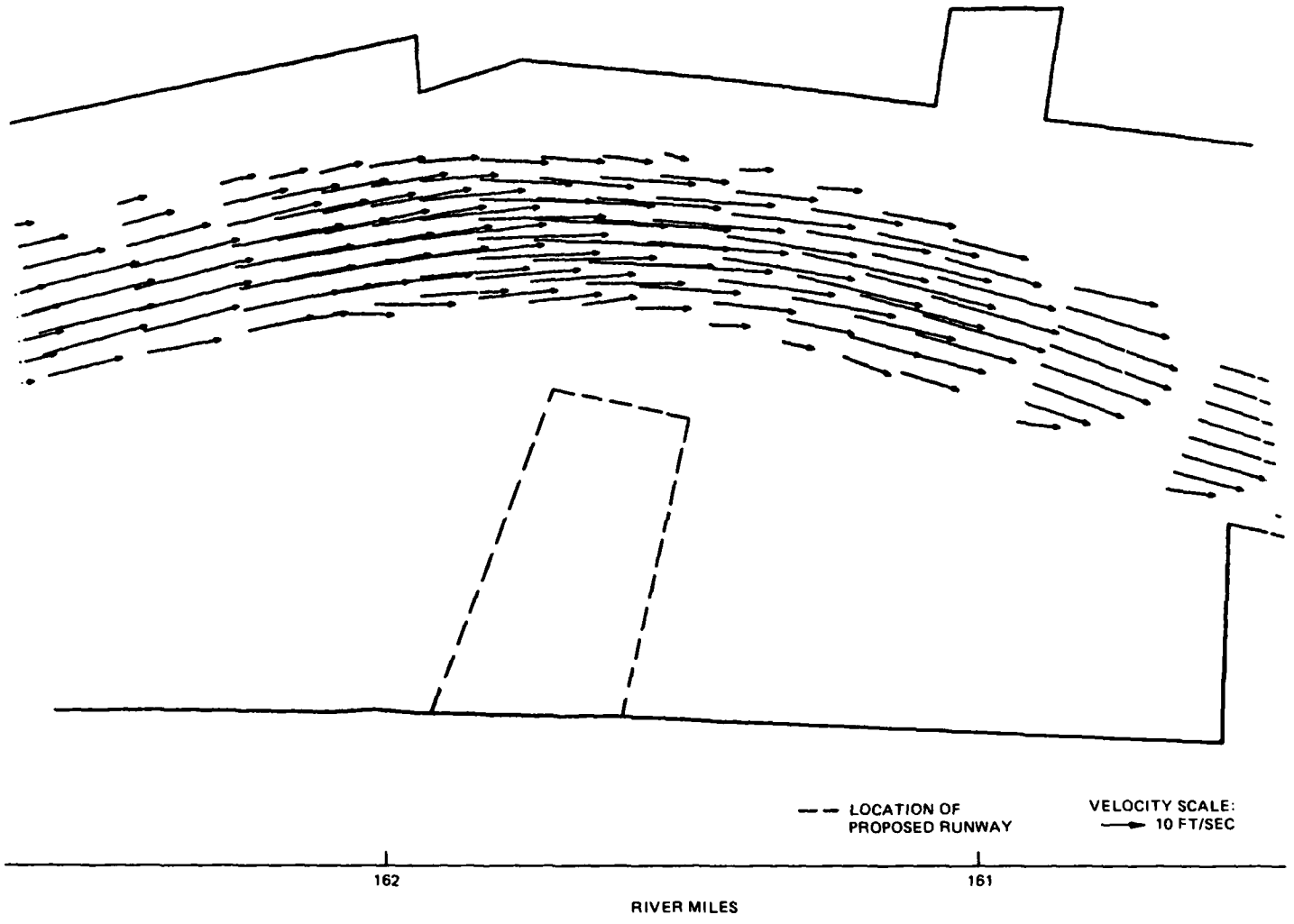


Figure 25. Magnification of flow pattern in navigation channel, base test

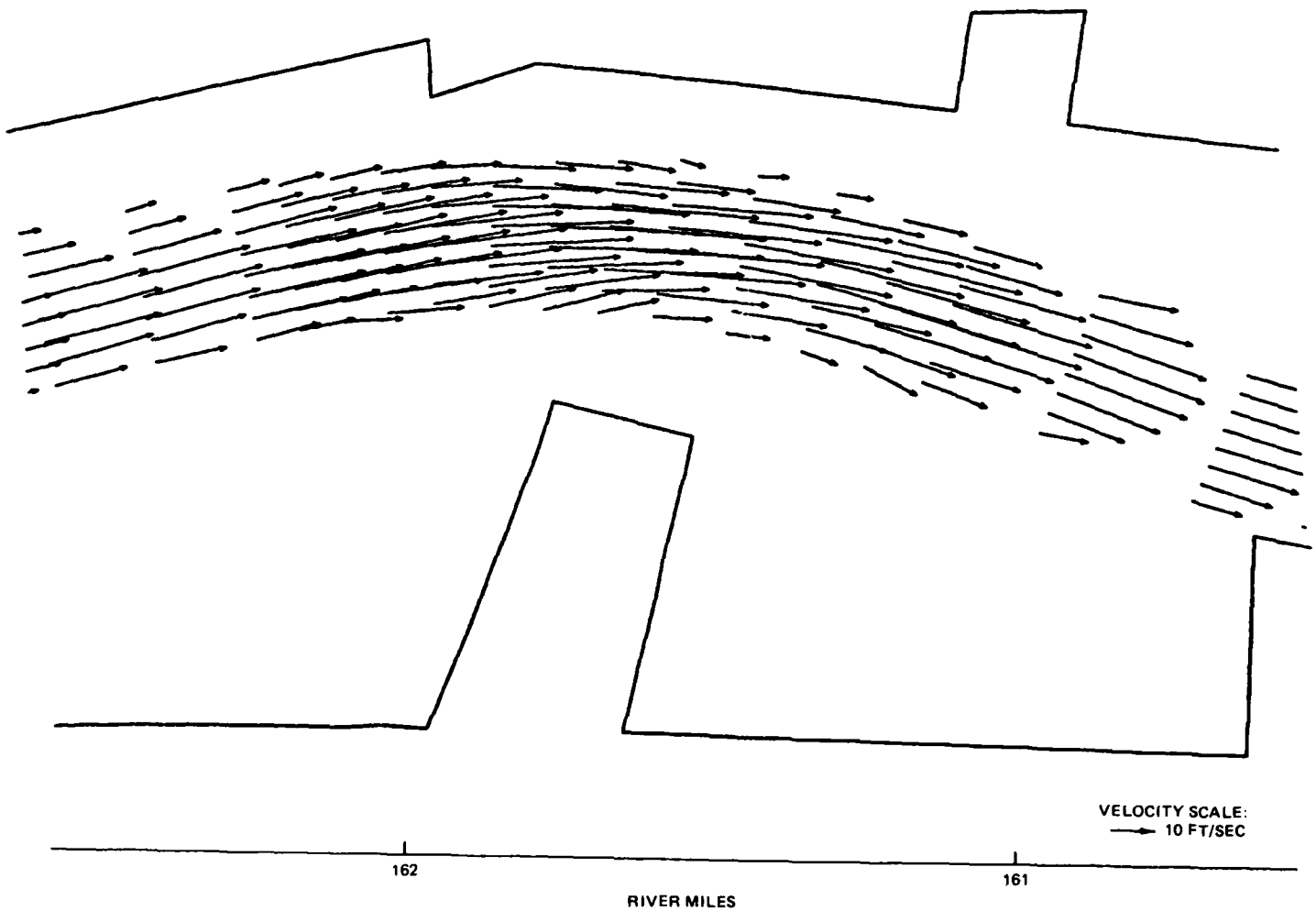


Figure 26. Magnification of flow pattern in navigation channel, plan test

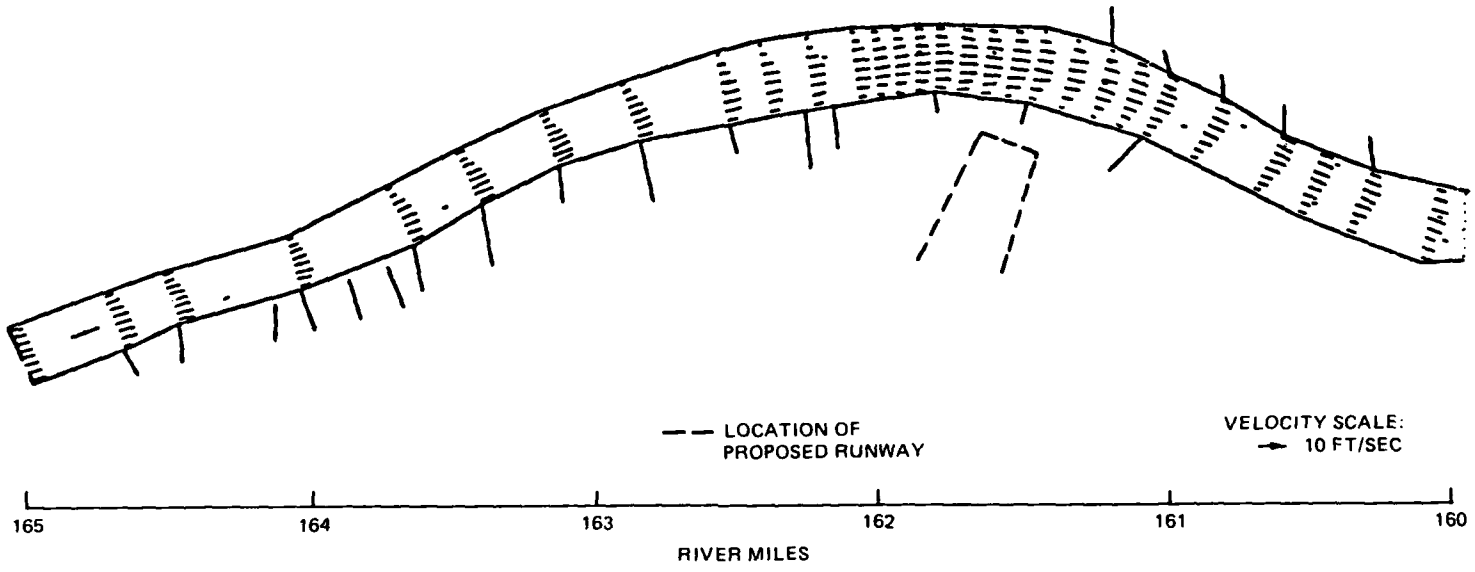


Figure 27. Navigation channel boundaries, base test

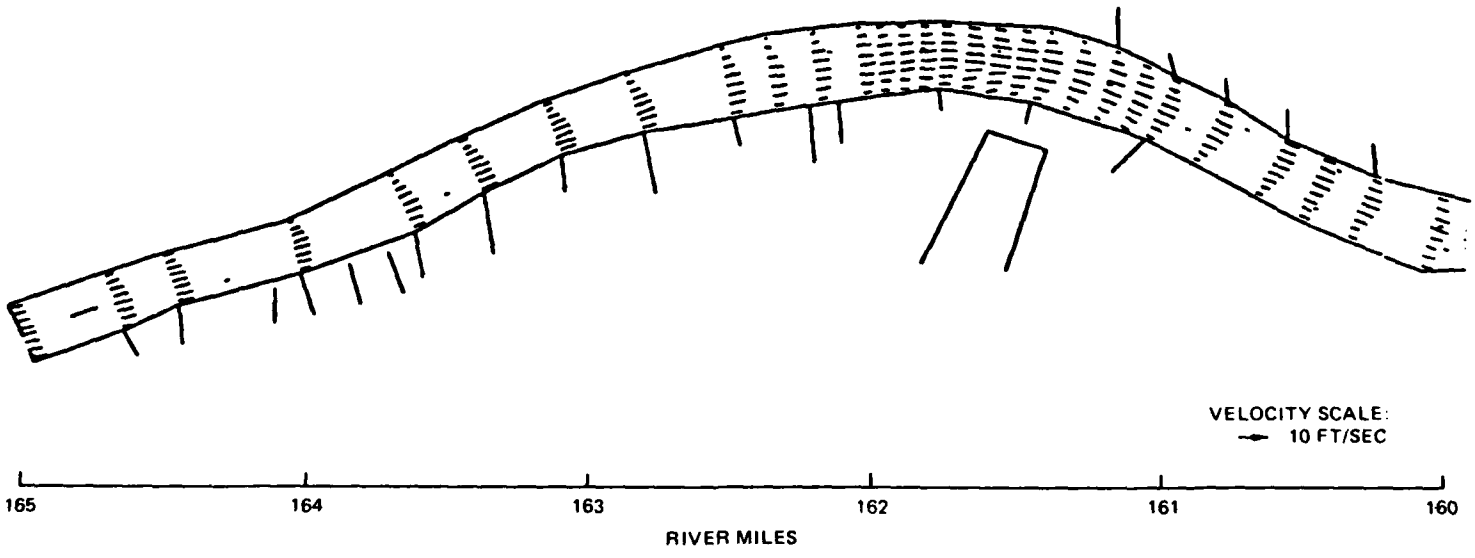


Figure 28. Navigation channel boundaries, plan test

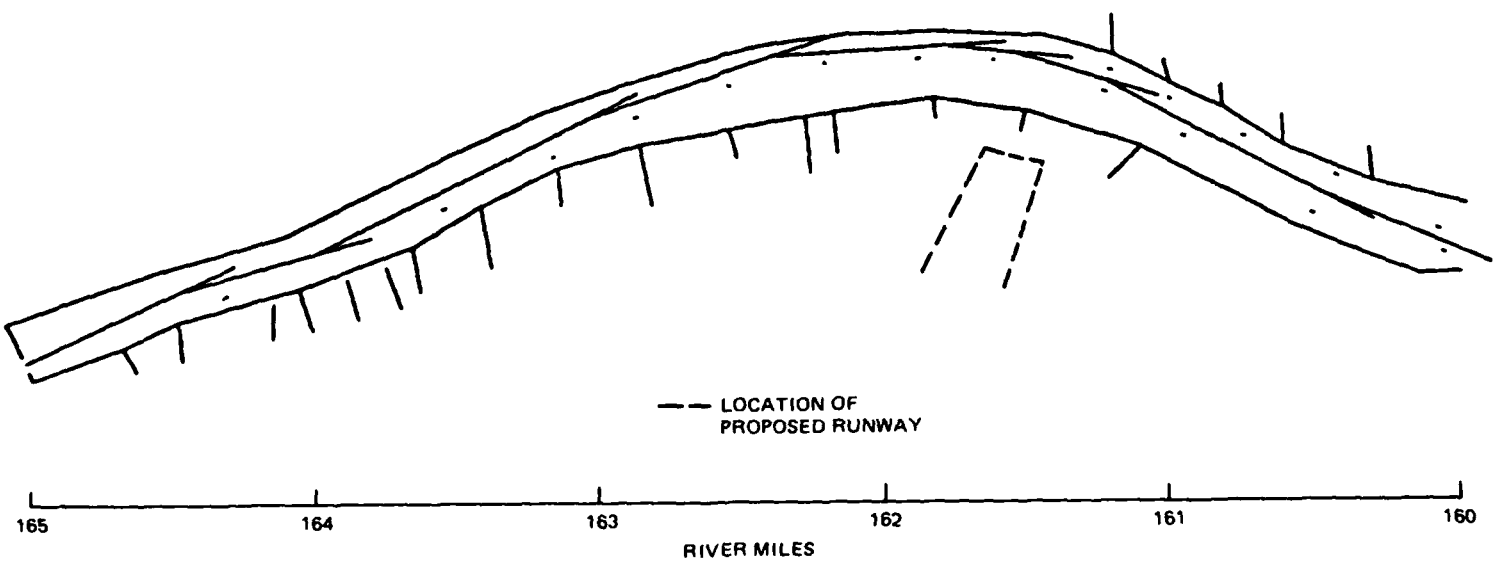


Figure 29. Autopilot track, base test

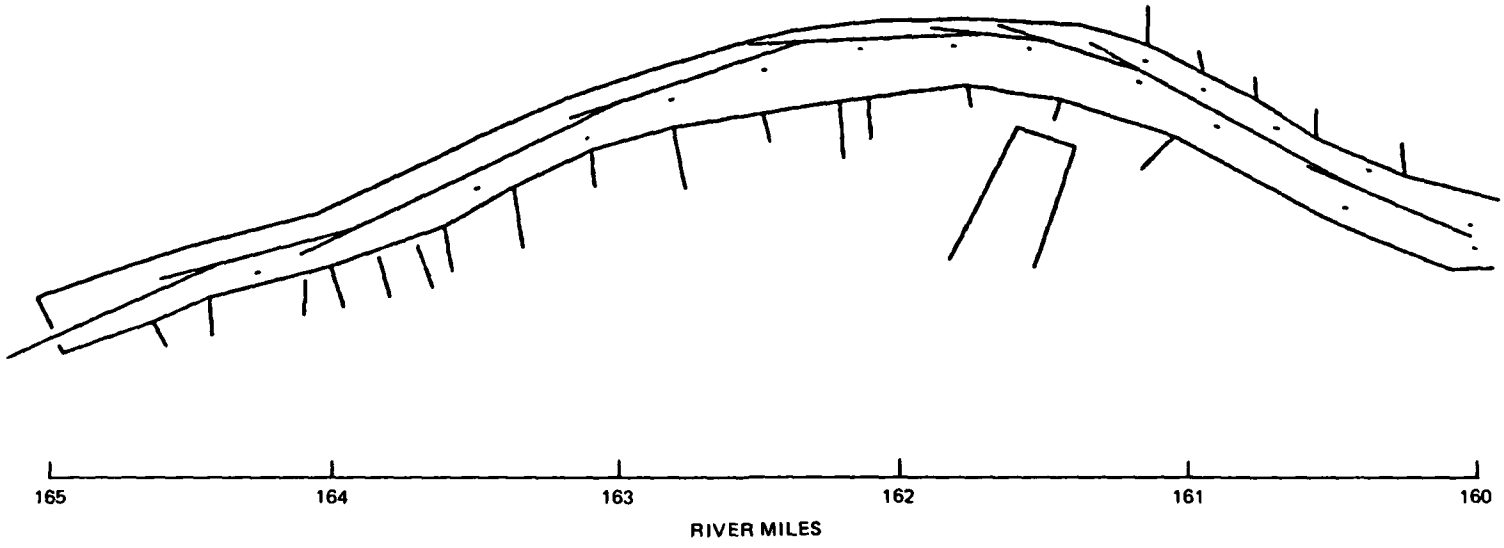


Figure 30. Autopilot track, plan test

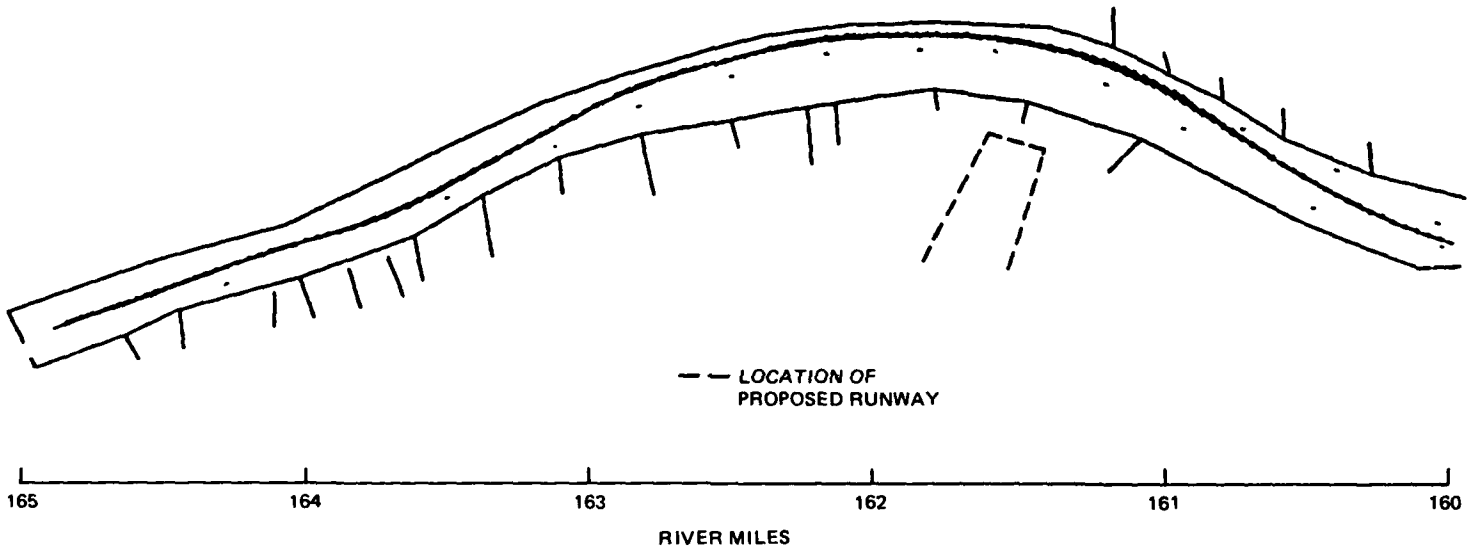


Figure 31. Transit path of downbound tow, base test

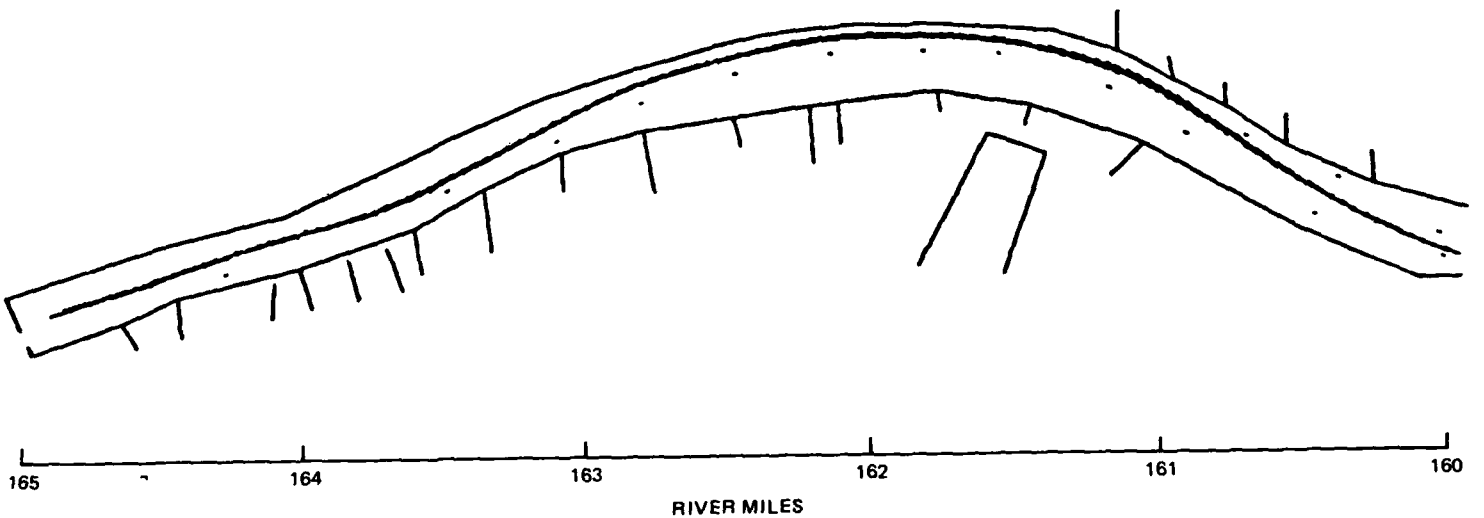


Figure 32. Transit path of downbound tow, plan test

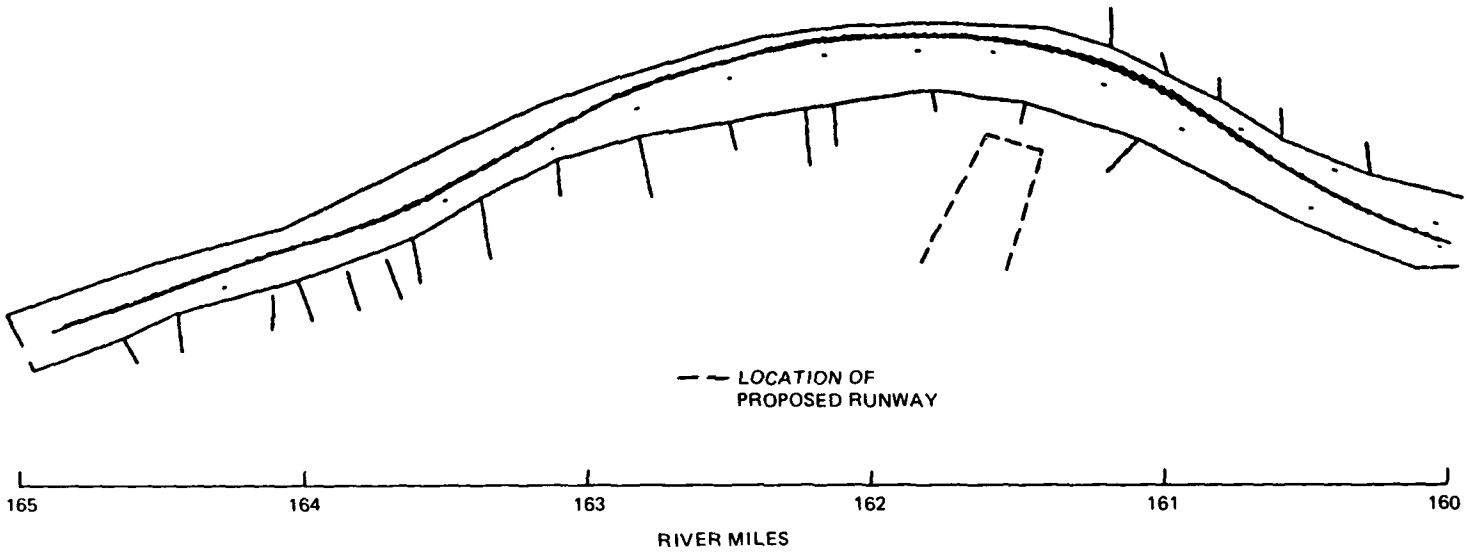


Figure 33. Upbound tow transit path, base test

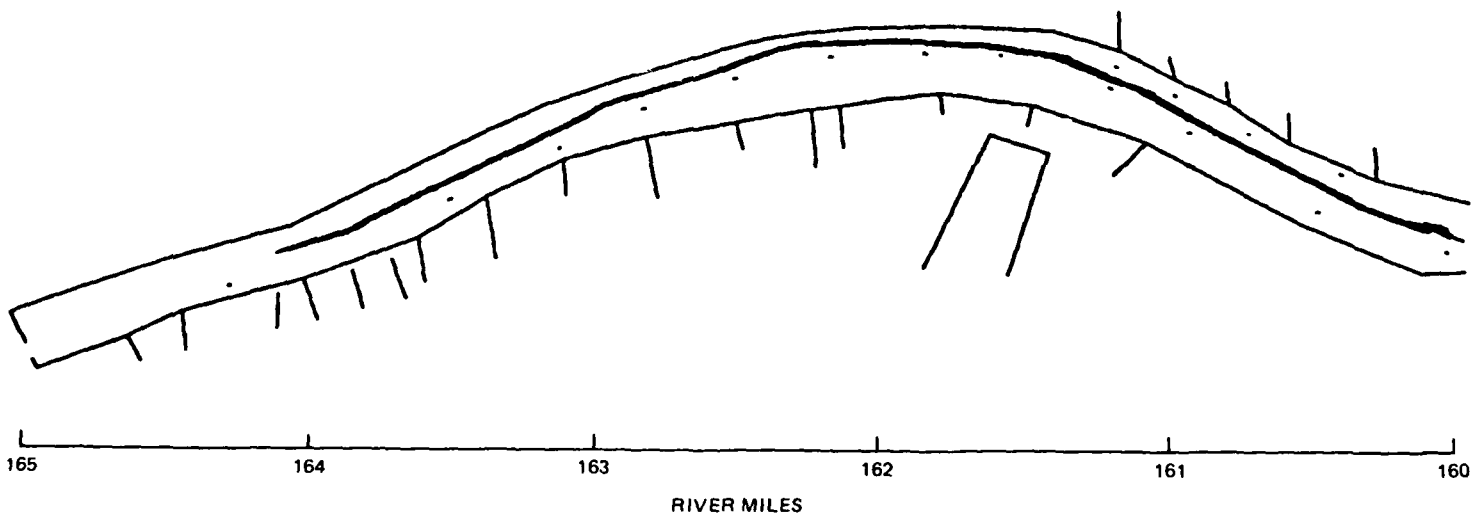


Figure 34. Upbound tow transit path, plan test

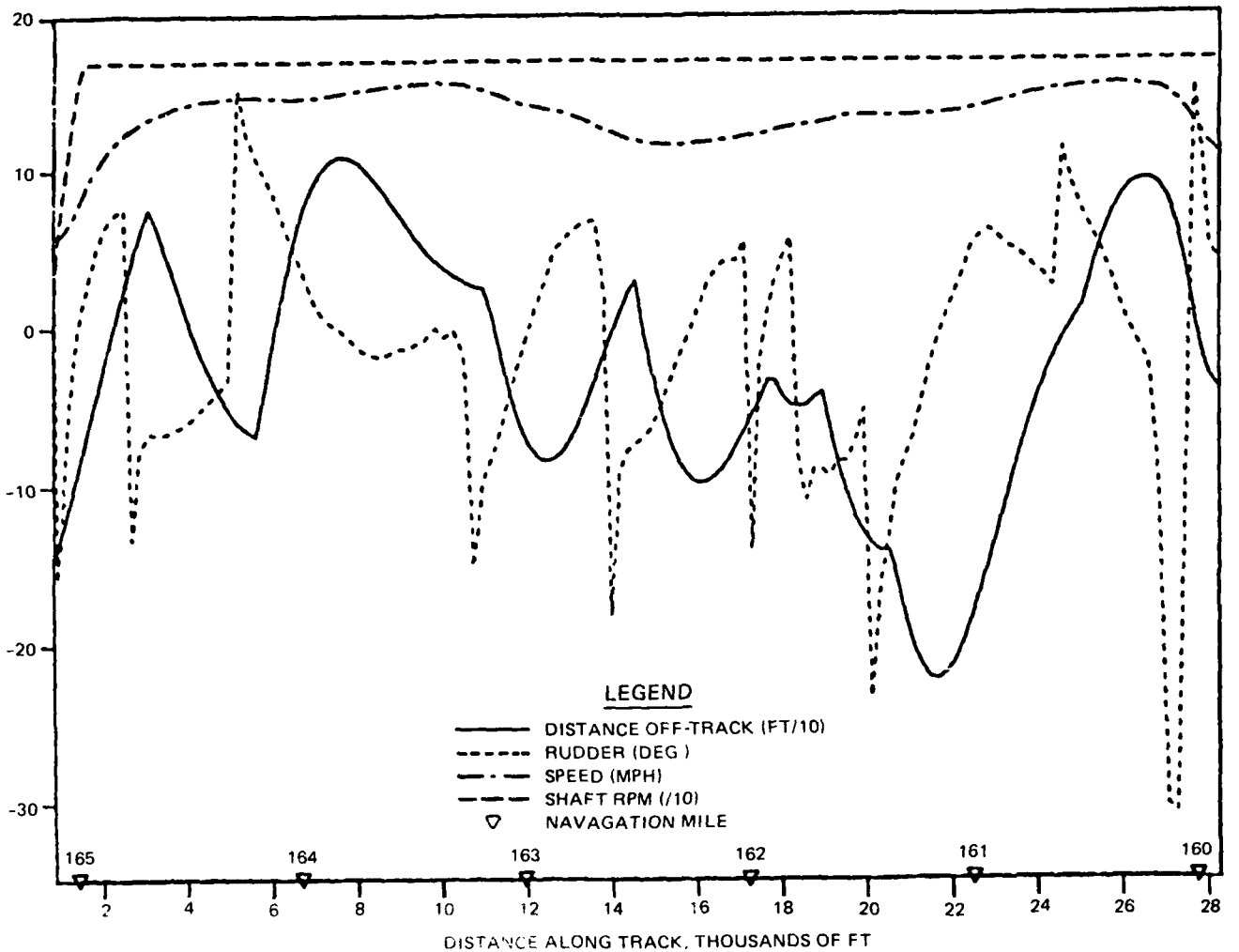


Figure 35. Transit recorder for downbound tow, base test

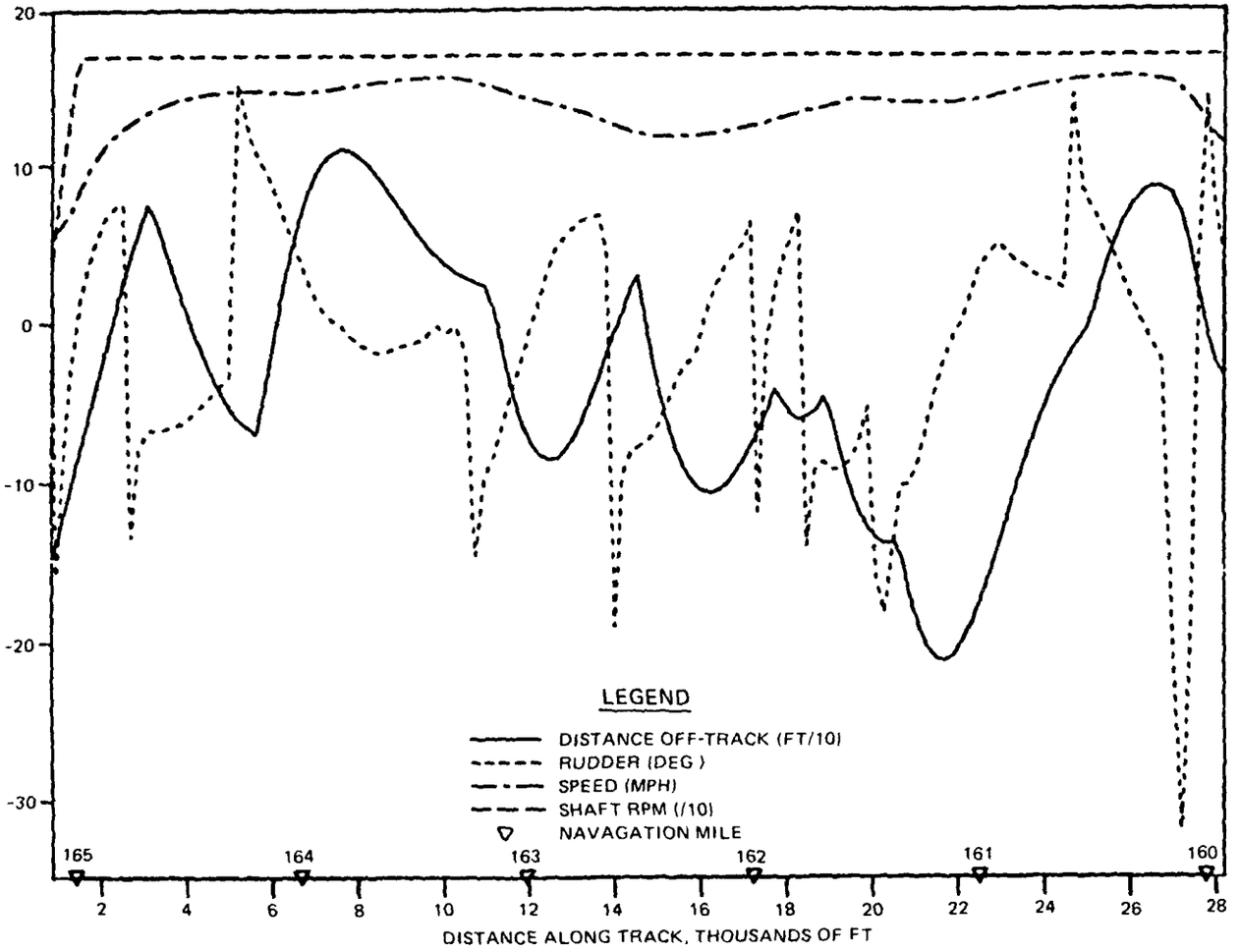


Figure 36. Transit recorder for downbound tow, plan test

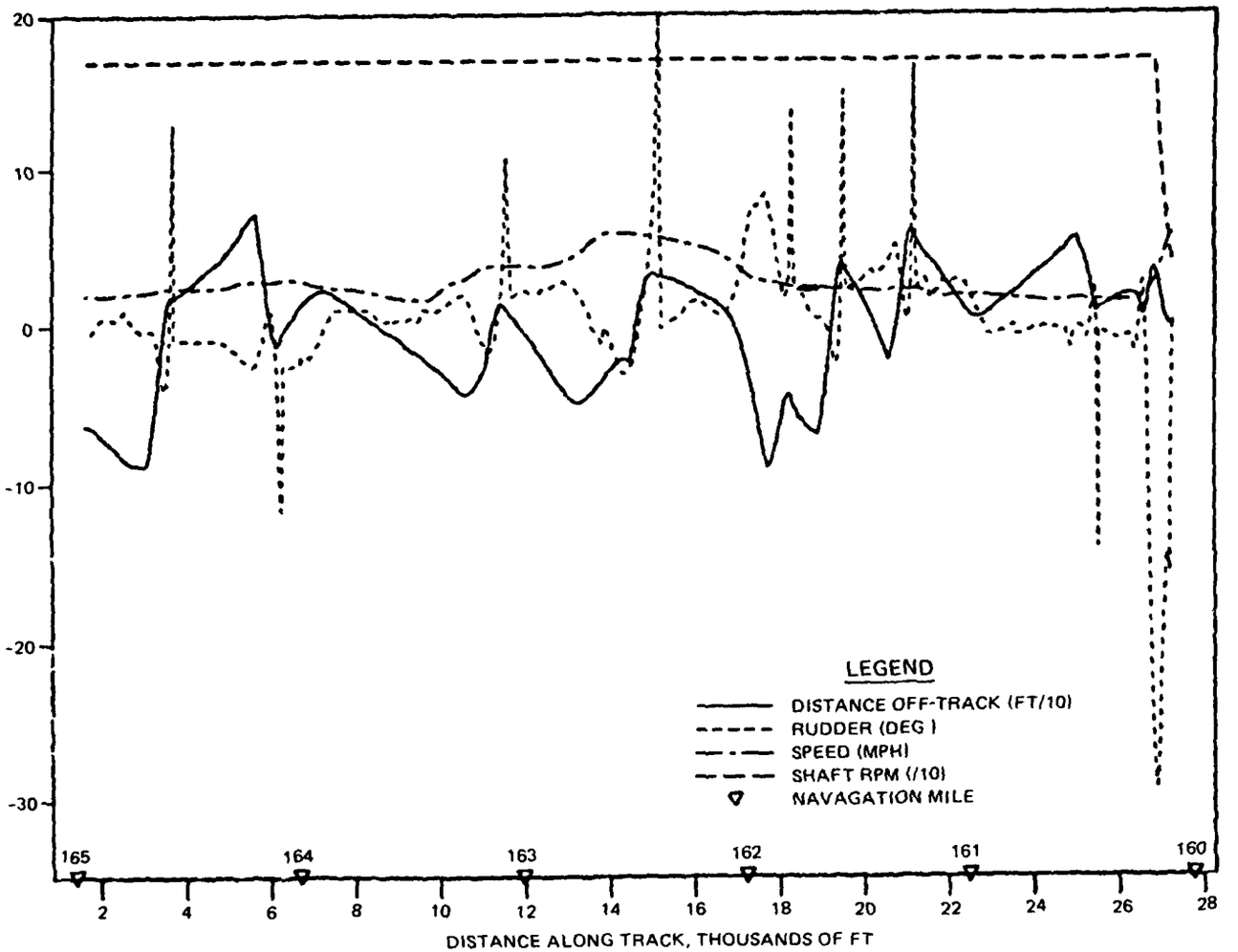


Figure 37. Transit recorder for upbound tows, base test

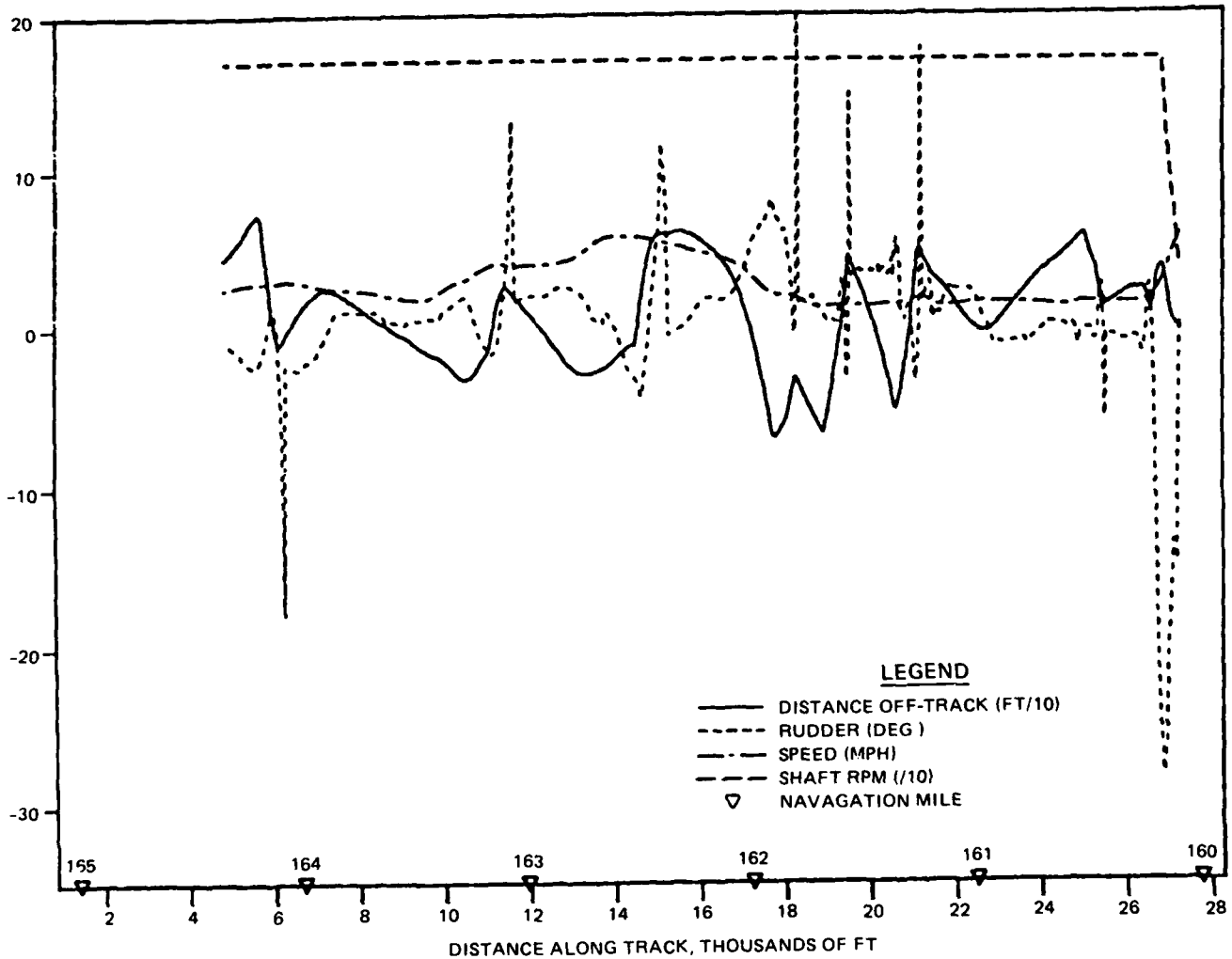


Figure 38. Transit recorder for upbound tows, plan test

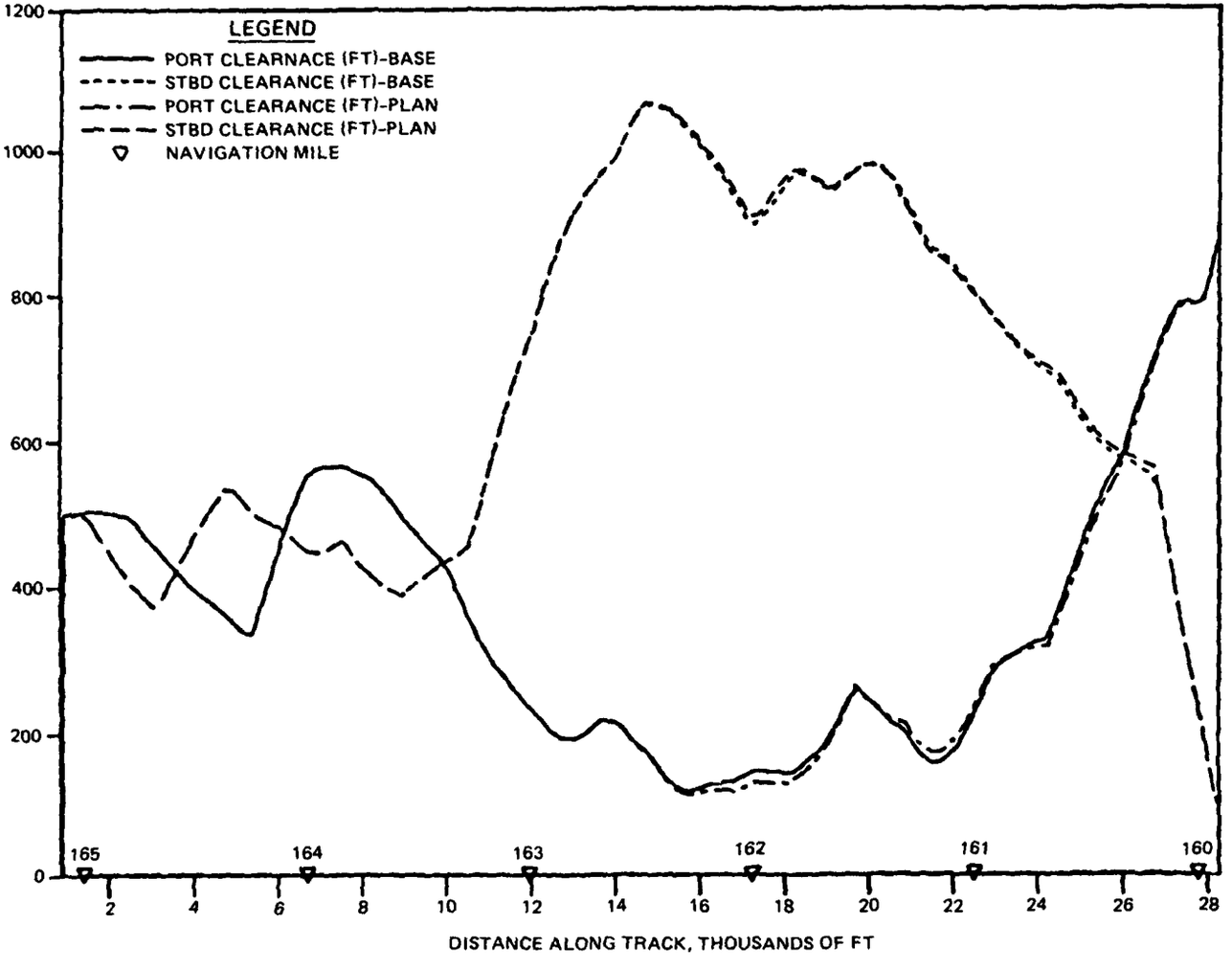


Figure 39. Tow clearance in the navigation channel, downbound tow

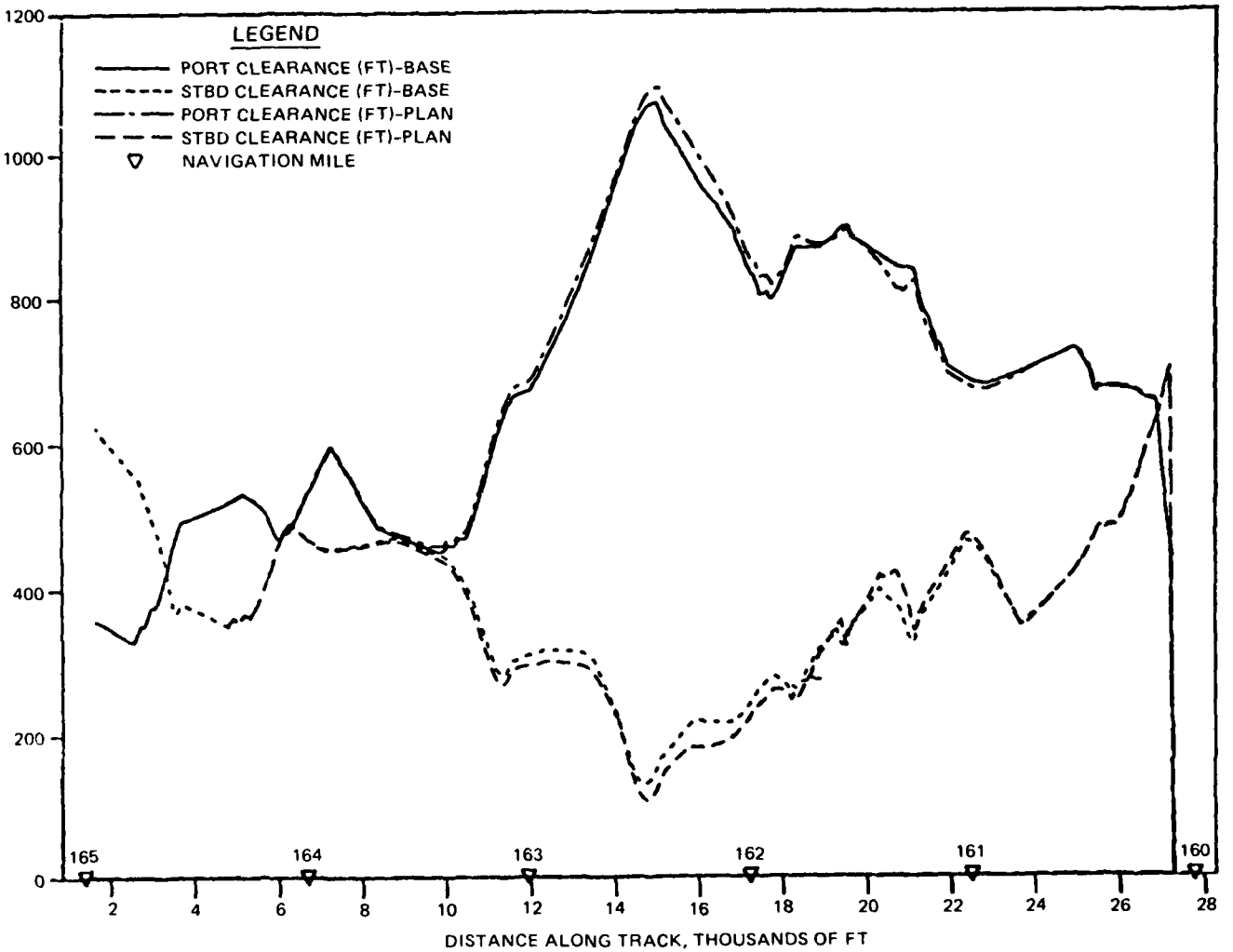


Figure 40. Tow clearance in the navigation channel, upbound tow

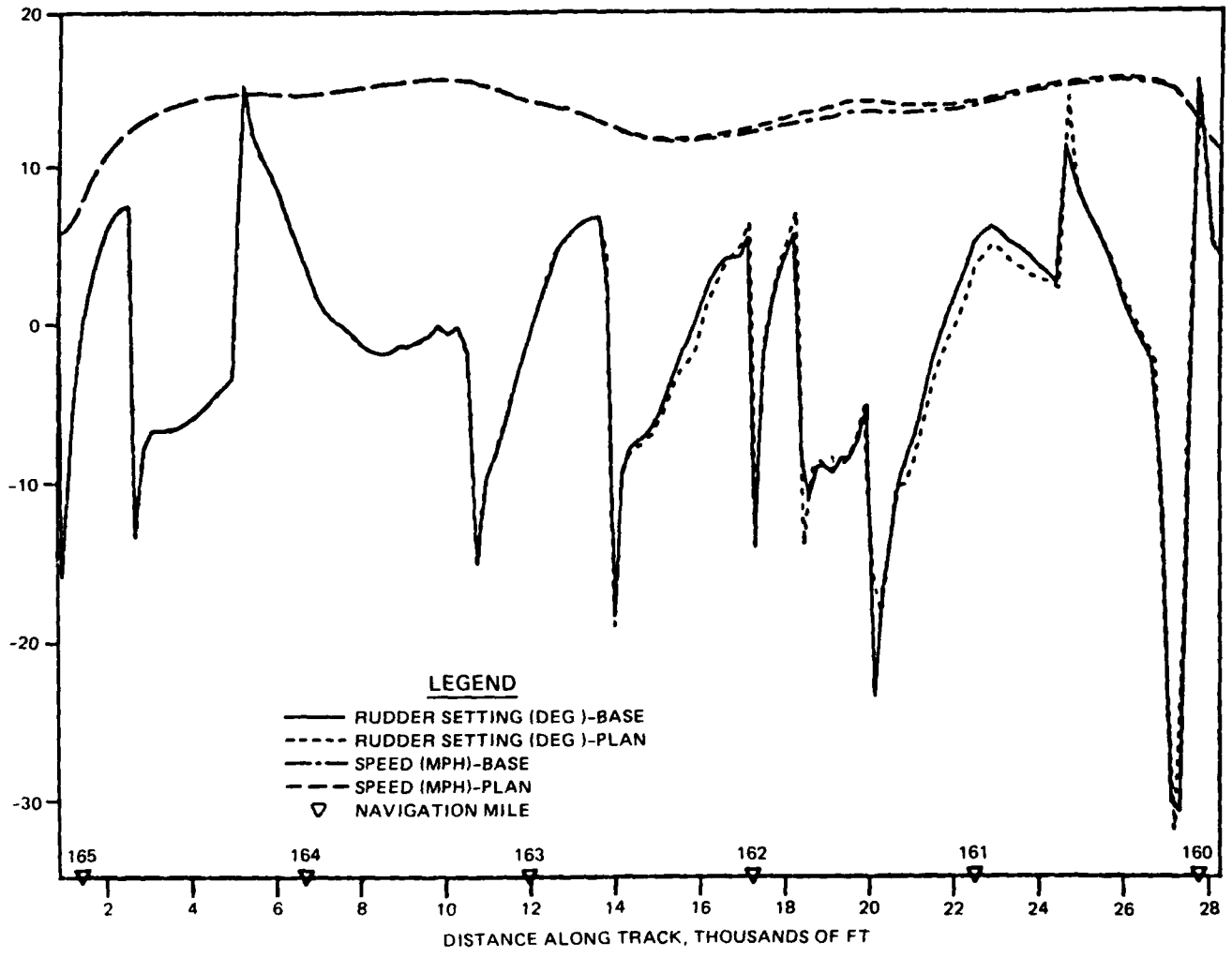


Figure 41. Rudder setting, downbound tow

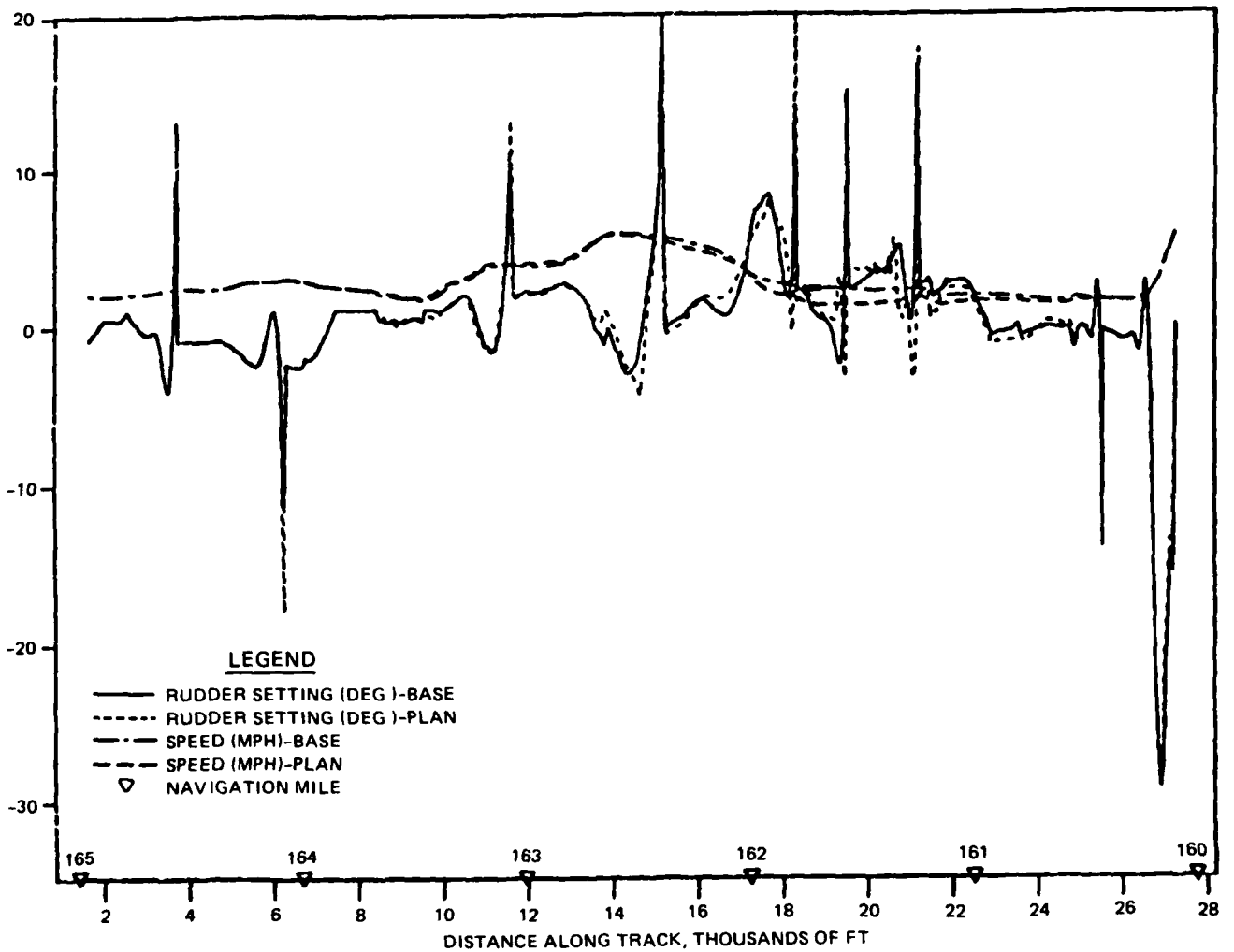


Figure 42. Rudder setting, upbound tow

# APPENDIX A: FINITE ELEMENT MODELING

1. The two numerical models used in this effort employ the finite element method to solve the governing equations. To help those who are unfamiliar with the method to better understand this report, a brief description of the method is given here. For a more thorough treatment, see Zienkiewicz (1971) or Desai (1979).

2. The finite element method approximates a solution to equations by dividing the area of interest into smaller subareas, which are called elements. The dependent variables (e.g., water-surface elevations and sediment concentrations) are approximated over each element by continuous functions which interpolate in terms of unknown point (node) values of the variables. An error, defined as the deviation of the approximation solution from the correct solution, is minimized. Then, when boundary conditions are imposed, a set of solvable simultaneous equations is created. The solution is smooth and continous over the area of interest.

3. In one-dimensional problems, elements are line segments. In two-dimensional problems, the elements are polygons, usually either triangles or quadrilaterals. Nodes are located on the edges of elements and occasionally inside the elements. The interpolating functions may be linear or higher order polynomials. Figure A1 illustrates a quadrilateral element with eight nodes and a linear solution surface.

4. Most water resource applications of the finite element method use the Galerkin method of weighted residuals to minimize error. In this method the residual, the total error between the approximate and correct solutions, is weighted by a function that is identical with the interpolating function and then minimized. Minimization results in a set of simultaneous equations in terms of nodal values of the dependent variable (e.g., water-surface elevations or sediment concentration). Time-dependent problems can have the time portion solved by the finite element methods, but it is generally more efficient to express derivatives with respect to time in finite difference form.

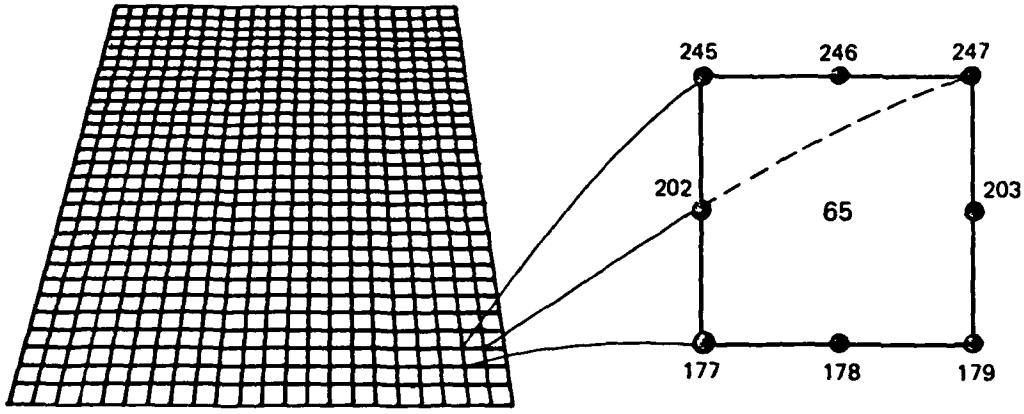


a. Eight nodes define each element

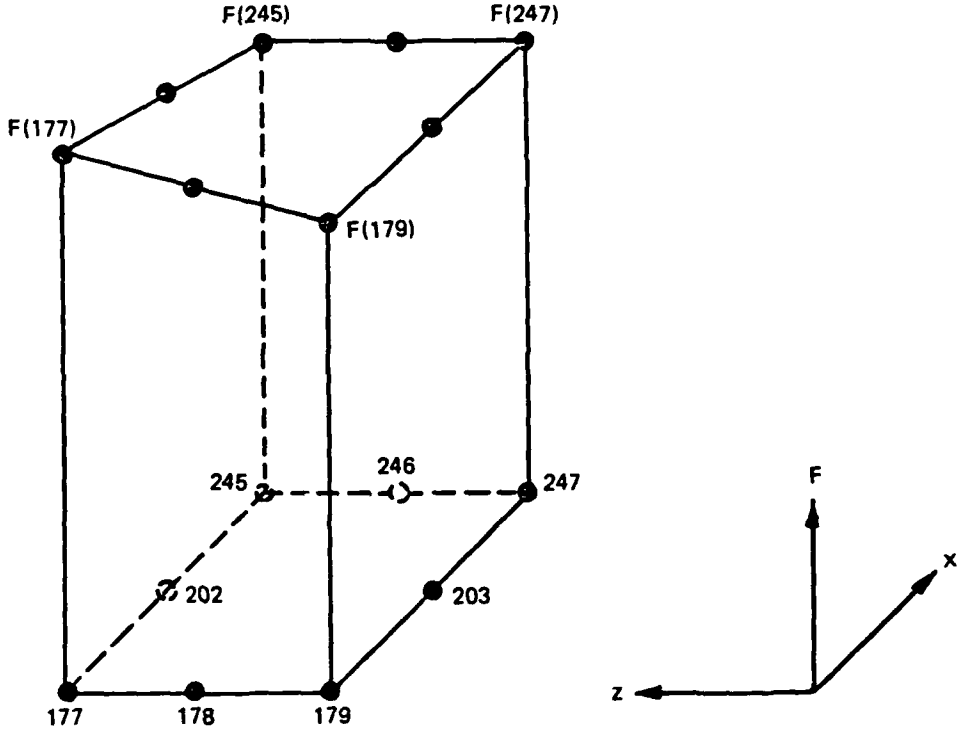


b. Linear interpolation function

Figure A1. Two-dimensional finite element mesh

## APPENDIX B: THE HYDRODYNAMIC MODEL, RMA-2V

1. The generalized computer program RMA-2 solves the depth-integrated equations of fluid mass and momentum conservation in two horizontal directions. The form of the solved equations is

$$\frac{\partial u}{\partial t} + u\frac{\partial u}{\partial x} + v\frac{\partial u}{\partial y} + g\frac{\partial h}{\partial x} + g\frac{\partial a_o}{\partial x} - \frac{\epsilon_{xx}}{\rho}\frac{\partial^2 u}{\partial x^2} - \frac{\epsilon_{xy}}{\rho}\frac{\partial^2 u}{\partial y^2}$$

$$-2v\omega \sin\phi + \frac{gu}{C^2 h}(u^2 + v^2)^{1/2} - \frac{\xi V_a^2}{h}\cos\Psi = 0 \qquad \text{(B1)}$$

$$\frac{\partial v}{\partial t} + u\frac{\partial v}{\partial x} + v\frac{\partial v}{\partial y} + g\frac{\partial h}{\partial y} + g\frac{\partial a_o}{\partial y} - \frac{\epsilon_{yx}}{\rho}\frac{\partial^2 v}{\partial x^2} - \frac{\epsilon_{yy}}{\rho}\frac{\partial^2 v}{\partial y^2} + 2\omega u \sin\phi$$

$$+ \frac{gv}{C^2 h}(u^2 + v^2)^{1/2} - \frac{\xi V_a}{h}\sin\Psi = 0 \qquad \text{(B2)}$$

$$\frac{\partial h}{\partial t} + \frac{\partial}{\partial x}(uh) + \frac{\partial}{\partial y}(vh) \qquad \text{(B3)}$$

where

$u$ = depth-integrated horizontal flow velocity in the x-direction

$t$ = time

$x$ = distance in the x-direction (longitudinal)

$v$ = depth-integrated horizontal flow velocity in the y-direction

$y$ = distance in the y-direction (lateral)

$g$ = acceleration due to gravity

$h$ = water depth

$a_o$ = elevation of the bottom

$\epsilon_{xx}$ = normal turbulent exchange coefficient in the x-direction

$\rho$ = fluid density

$\epsilon_{xy}$ = tangential turbulent exchange coefficient in the x-direction

$\omega$ = angular rate of earth's rotation

$\Phi$ = latitude

$C$ = Chezy roughness coefficient

$\xi$ = coefficient relating wind speed to stress exerted on the fluid

$V_a$ = wind velocity

$\Psi$ = angle between wind direction and x-axis

$\varepsilon_{yx}$ = tangential turbulent exchange coefficient in the y-direction

$\varepsilon_{yy}$ = normal turbulent exchange coefficient in the y-direction

2. The Chezy roughness formulation of the original code was modified in the input portion so that Manning's n roughness coefficients may be specified from input Manning's n values and initial water depth.

3. Equations B1, B2, and B3 are solved by the finite element method using Galerkin weighted residuals. The elements may be either quadrilaterals or triangles and may have curved (parabolic) sides. The shape functions are quadratic for flow and linear for depth. Integration in space is performed by Gaussian integration. Derivatives in time are replaced by a nonlinear finite difference approximation. Variables are assumed to vary over each time interval in the form

$$f(t) = f(o) + at + bt^c \qquad t_o \leq t < t_1 \tag{B4}$$

which is differentiated with respect to time, and cast in finite difference form. Letters a , b , and c are constants. It has been found by experiment that the best value for c is 1.5 (Norton and King 1977).

4. The solution is fully implicit and the set of simultaneous equations is solved by Newton-Raphson iteration. The computer code executes the solution by means of a front-type solver that assembles a portion of the matrix and solves it before assembling the next portion of the matrix. The front solver's efficiency is largely independent of bandwidth and thus does not require as much care in formation of the computational mesh as do traditional solvers.

5. The code RMA-2V is based on the earlier version RMA-2 (Norton and King 1977) but differs from it in several ways. First, it is formulated in terms of velocity (v) instead of unit discharge (vh), which improves some aspects of the code's behavior; it permits drying and wetting of areas within the grid; and it permits specification of turbulent exchange coefficients in directions other than along the x- and y-axis.

## APPENDIX C: THE SEDIMENT TRANSPORT MODEL, STUDH

1. The generalized computer program STUDH solves the depth-integrated convection-dispersion equation in two horizontal dimensions for a single sediment constituent. The form of the solved equation is

$$\frac{\partial C}{\partial t} + u \frac{\partial C}{\partial x} + v \frac{\partial C}{\partial y} = \frac{\partial}{\partial x} D_x \frac{\partial C}{\partial x} + \frac{\partial}{\partial y} D_y \frac{\partial C}{\partial y} + \alpha_1 C + \alpha_2 \qquad \text{(C1)}$$

where

$C$ = concentration of sediment

$u$ = depth-integrated velocity in x-direction

$v$ = depth-integrated velocity in y-direction

$D_x$ = dispersion coefficient in x-direction

$D_y$ = dispersion coefficient in y-direction

$\alpha_1$ = coefficient of concentration dependent source/sink term

$\alpha_2$ = coefficient of source/sink term

STUDH is related to the generalized computer program SEDIMENT II (Ariathurai, MacArthur, and Krone 1977) developed at the University of California, Davis, under the direction of R. B. Krone. STUDH is the product of joint efforts of WES personnel (under the direction of W. A. Thomas) and R. Ariathurai, now a member of Resource Management Associates.

2. The source/sink terms in Equation C1 are computed in routines that treat the interaction of the flow and the bed. Separate sections of the code handle computations for clay bed and sand bed problems. In the tests described here, only sand beds were considered. The source/sink terms were evaluated by first computing a potential sand transport capacity for the specified flow conditions, comparing that capacity with the amount of sand actually being transported, and then eroding from or depositing to the bed at a rate that would approach the equilibrium value after sufficient elapsed time.

3. The potential sand transport capacity in these tests was computed by the method of Ackers and White (1973), which uses a transport power (work rate) approach. It has been shown to provide superior results for transport under steady-flow conditions (White, Milli, and Crabbe 1975) and for combined waves and currents (Swart 1976). WES flume tests have shown that the concept is valid for transport by estuarine currents.

4. The total load transport function of Ackers and White is based upon a dimensionless grain size

$$D_{gr} = D \left[ \frac{g(s - 1)}{\nu^2} \right]^{1/3} \tag{C2}$$

where

$D$ = sediment particle diameter

$g$ = acceleration due to gravity

$s$ = specific gravity of the sediment

$\nu$ = kinematic viscosity of the fluid

and a sediment mobility parameter

$$F_{gr} = \left[ \frac{\tau^n \tau'^{(1-n)}}{\rho g D(s - 1)} \right]^{1/2} \tag{C3}$$

where

$\tau$ = total boundary shear stress

$n$ = a coefficient expressing the relative importance of bed-load and suspended-load transport, given in Equation C5

$\tau'$ = boundary surface shear stress

$\rho$ = water density

The surface shear stress is that part of the total shear stress which is due to the rough surface of the bed only, i.e., not including that part due to bed forms and geometry. It therefore corresponds to that shear stress which a plane bed would exert on the flow.

5. The total sediment transport is expressed as a potential concentration

$$G_p = k \left( \frac{F_{gr}}{A} - 1 \right)^m \frac{sD}{h} \left( \sqrt{\frac{\rho}{\tau}} U \right)^n \tag{C4}$$

where $U$ is the average flow velocity, $h$ is the water depth, and $k$, $m$, and $A$ are coefficients as defined below. For $1 < D_{gr} \leq 60$

$$n = 1.00 - 0.56 \log D_{gr} \tag{C5}$$

$$A = \frac{0.23}{\sqrt{D_{gr}}} + 0.14 \tag{C6}$$

$$\log C = 2.86 \log D_{gr} - (\log D_{gr})^2 - 3.53 \tag{C7}$$

$$m = \frac{9.66}{D_{gr}} + 1.34 \tag{C8}$$

For $D_{gr} > 60$

$$n = 0.00 \tag{C9}$$

$$A = 0.17 \tag{C10}$$

$$k = 0.025 \tag{C11}$$

$$m = 1.5 \tag{C12}$$

6. Bed shear stresses for combined waves and currents are calculated by STUDH using the equation

$$\tau'_{wc} = \left(\frac{f_w u_{om} + f_c U}{u_{om} + U}\right) \frac{\rho}{2} \left(U + \frac{u_{om}}{2}\right)^2 \tag{C13}$$

for surface shear stress (plane beds) and

$$\tau_{wc} = \frac{1}{2} f_c \rho U^2 + \frac{1}{4} f_w \rho u_{om}^2 \tag{C14}$$

for total shear stress, where

$f_w$ = shear stress coefficient for waves

$f_c$ = shear stress coefficient for currents

$U$ = average flow velocity

$u_{om}$ = maximum wave orbital velocity near the bed

$\rho$ = density of water

Equations C13 and C14 are based on the work of Jonsson (1966), and Bijker and Swart (Swart 1976). Development of the equations is given by McAnally and Thomas (1981).

7. Using Equations C13 and C14 for shear stresses in the Ackers-White equations (Equations C2-C12) results in a potential sediment concentration, $G_p$. This value is the depth-averaged concentration of sediment that will occur if an equilibrium transport rate is reached with a nonlimited supply of sediment. The rate of sediment deposition (or erosion) is then computed as

$$R = \frac{G_p - C}{t_c} \tag{C15}$$

where

$C$ = present sediment concentration

$t_c$ = time constant

For deposition, the time constant is

$$t_c = \text{larger of} \begin{cases} \Delta t \\ \text{or} \\ \dfrac{C_{Ld} h}{V_s} \end{cases} \tag{C16}$$

and for erosion it is

$$t_c = \text{larger of} \begin{cases} \Delta t \\ \text{or} \\ \dfrac{C_{Le} h}{U} \end{cases} \tag{C17}$$

where

$\Delta t$ = computational time-step

$C_{Ld}$ = response time coefficient for deposition

$h$ = water depth

$V_s$ = sediment settling velocity

$C_{Le}$ = response time coefficient for erosion

U = average current speed

8. Equation C1 is solved by the finite element method using Galerkin weighted residuals. Like RMA-2V, which uses the same general solution technique, elements are quadrilateral and may have parabolic sides. Shape functions are quadratic. Integration in space is Gaussian. Time-stepping is performed by a Crank-Nicholson approach with a weighting factor (theta) of 0.66. The solution is fully implicit and front-type solver is used similar to that in RMA-2V.

# APPENDIX D: THE NAVIGATION MODEL

1. The effects of the proposed runway extension on navigation operations through the study reach were studied using a ship hydrodynamics model developed for use in modeling shallow-draft pushtows. The model was developed by Hydronautics, Inc., and is incorporated into the WES ship/tow simulator facility. This model is a mathematical model for the maneuvering of a river tow and consists of the coupled differential equations of motion in three degrees of freedom (surge, yaw, and sway) in the X,Y plane and the complete set of hydrodynamic coefficients and external forces which are required in order to numerically integrate these equations. There are also auxiliary equations that describe the response of the steering and propulsion system to command signals.

2. A complete set of three coupled differential equations with all of the necessary terms to simulate normal maneuvers of surface ships is presented in Goodman et al. (1976) and a description of the application of these equations to the towboat simulator is given by Miller (1979). These equations have been used successfully for a number of years to calculate the maneuver trajectories for a wide range of surface ship types in deep and shallow water. These equations have been modified to account for maneuvering characteristics that are unique to river tows. A right-hand orthogonal system of moving axes, fixed in the body, with its origin normally located at the center of mass of the body is used for reference. The positive direction of the axes, angles, linear velocity components, angular velocity components, forces, and moments are given in Figure D1. The numerical values for the hydrodynamic coefficients used in the equations are written in terms of the complete barge flotilla/towboat configuration and are nondimensional. Thus the values of the coefficients can be applied to geometrically similar tows. The values of the coefficients embrace the interaction effects between the rudder and hull, propeller and hull, and propeller and rudder as determined from towing tank model tests of the complete configuration.

3. An important consideration in the maneuvering of a river tow is the effect of current which can vary significantly along the length of the tow. As a result, it is necessary to introduce the effect of the current velocity into the mathematical model. The approach adopted was to define the hydrodynamic terms in the equations based on the relative velocities and yaw rate between

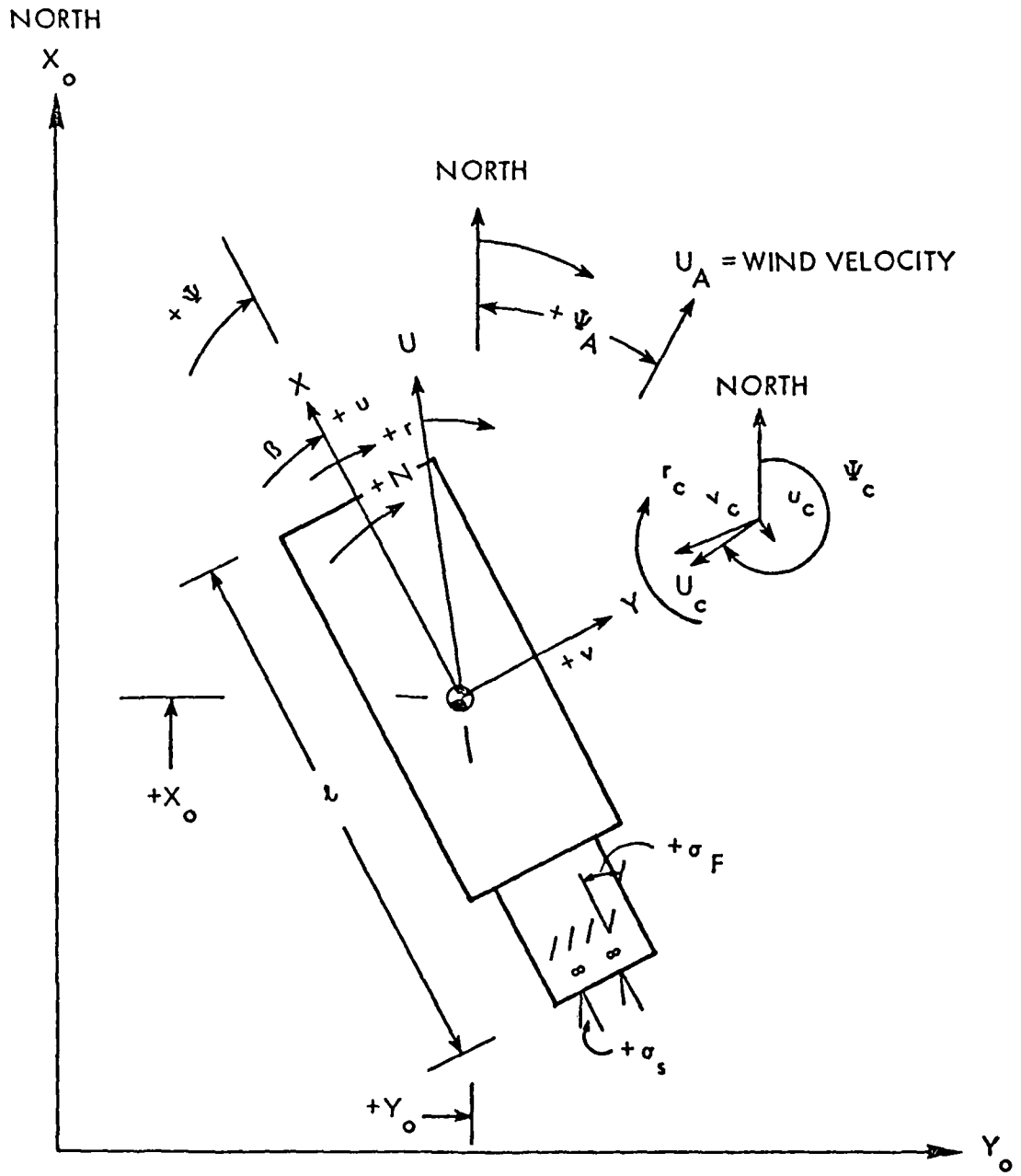


Figure D1. Sign convention for river tow maneuvering simulation

the hull and the fluid rather than the inertial velocities and yaw rate. The relative velocities and relative yaw rate can be calculated by the vector addition of the inertial velocity and inertial yaw rate and the current velocities and the current yaw rate. In the numerical integration, the procedure is to define a matrix of current speeds and directions at points on the X,Y plane. Based on the location of the bow, midship, and stern of the tow, an interpolation in the current speed and direction matrix is carried out to obtain the current speed and direction at the bow, midship, and stern. Then a mean longitudinal and lateral current velocity in the body axis system is computed as the average of the values at the bow, midship, and stern. The variation of the lateral velocity along the tow is accounted for by the apparent current yaw rate defined by the difference in the lateral velocities at the bow and stern divided by the tow length. This accounts for variations.

4. Towboat propulsion systems differ from those in ships. Tows perform backing operations frequently, and because of this, they have two sets of rudders. Thus terms are included to account for the forces and moments created by the flanking and steering rudders which can be operated independently. In addition, many tows are propelled with twin propellers that are independently powered. Terms have been included for twin propeller forces and moments which may operate at different rpm's and different directions of rotation.

5. In realistic maneuvers, river tows operate both ahead and astern and in some cases at large drift angles. In order to properly represent the hydrodynamic forces and moments which act in such conditions, different sets of hydrodynamic coefficients are used depending on the relative drift angle. Thus the hydrodynamic coefficients vary depending on whether the motion is ahead or astern and whether the drift angle is near 90 or 270 deg.

6. In addition, tows often operate in shallow water and near banks. In shallow-water operations, the tow maneuvering characteristics change significantly--cypically becoming more stable and thus less maneuverable. Adjustments are made to the hydrodynamic coefficients to reflect these changes and, like the determination of the deepwater hydrodynamic coefficients, are developed from model tests at various depth-to-draft ratios. Bank forces are a function of the distance from and the orientation to the banks. Computations for the bank forces and moments are included in the hydrodynamic equations.

7. The equations of motion are solved stepwise in time in the computer program. At each time-step, the current velocity, depth of water, and distance

from the port and starboard bank are determined at the bow, midship, and stern of the tow. Currents and depths are entered to the model as cross sections with up to 30 cross sections and 8 points per cross section being allowed. Port and starboard bank conditions are defined for each cross section by specifying the overbank depth and slope of the bank.

# APPENDIX E: REFERENCES


Ackers, P., and White, W. R. 1973 (Nov). "Sediment Transport: New Approach and Analysis," Journal, Hydraulics Division, American Society of Civil Engineers, No. HY11.

Ariathurai, R., MacArthur, R. D., and Krone, R. C. 1977 (Oct). "Mathematical Model of Estuarial Sediment Transport," Technical Report D-77-12, US Army Engineer Waterways Experiment Station, Vicksburg, Miss.

Chow, Ven Te. 1959. Open-Channel Hydraulics, McGraw-Hill, New York, N. Y. pp. 109-123.

Desai, C. S. 1979. Elementary Finite Element Method, Prentice-Hall, Englewood Cliffs, N. J.

Garver and Garver, Inc. 1977 (Apr). East Belt Freeway Arkansas River Bridge: Preliminary Report, Little Rock, Ark.

Goodman, Alex, et al. 1976 (Jun). "Experimental Techniques and Methods of Analysis Used at Hydronautics for Surface Ship Maneuvering Predictions," Hydronautics, Incorporated, Technical Report 7600-1.

Jonsson, I. G. 1966. "The Friction Factor for a Current Superimposed by Waves," Basic Research Progress Report No. 11, Technical University of Denmark, Copenhagen.

McAnally, W. H., Jr., and Thomas, W. A. "Shear Stress Computations in a Numerical Model for Estuarine Sediment Transport" (in preparation), US Army Engineer Waterways Experiment Station, Vicksburg, Miss.

Miller, Eugene R., Jr. 1979 (May). "Towboat Maneuvering Simulator - Theoretical Description," Hydronautics, Incorporated, Technical Report 7909-1, Volume III.

Norton, W. R., and King, I. P. 1977 (Feb). "Operating Instructions for the Computer Program RMA-2V," Resource Management Associates, Lafayette, Calif.

US Army Corps of Engineers, Little Rock District. 1960 (May). Project Design Memorandum No. 5 - 3: Navigation Channel and Appurtenances, Normal Pool Elevations and Dam Sites.

Swart, D. H. 1976 (Sep). "Coastal Sediment Transport, Computation of Longshore Transport," R968, Part 1, Delft Hydraulics Laboratory, The Netherlands.

White, W. R., Milli, H., and Crabbe, A. D. 1975. "Sediment Transport Theories: An Appraisal of Available Methods," Report Int 119 (Vols 1 and 2), Hydraulics Research Station, Wallingford, England.

Zienkiewicz, O. C. 1971. The Finite Element Method in Engineering Science, McGraw-Hill, London.

END

FILMED

7-85

DTIC